Received: 1 January 2023 | Revised: 10 May 2023 | Accepted: 30 July 2023

DOI: 10.1002/ldr.4865

RESEARCH ARTICLE

WILEY

Quantification of short-term transformations of proglacial landforms in a temperate, debris-charged glacial landsystem, Kviárjökull, Iceland

Szymon Śledź[1] | Marek W. Ewertowski[1,2] | David J. A. Evans[3]

[1]Faculty of Geographical and Geological Sciences, Adam Mickiewicz University, Poznań, Poland

[2]School of Earth and Environment, University of Canterbury, Christchurch, New Zealand

[3]Department of Geography, Durham University, Durham, UK

Correspondence
Szymon Śledź, Faculty of Geographical and Geological Sciences, Adam Mickiewicz University, Krygowskiego 10, 61-680 Poznań, Poland.
Email: szysle@amu.edu.pl

Funding information
Narodowe Centrum Nauki, Grant/Award Number: 2019/35/B/ST10/03928

Abstract

Proglacial areas are dynamic landscapes and important indicators of geomorphic changes related to climate warming. Systematic and repeat surveys of landforms presently evolving on glacier forelands facilitate the quantification of rates of change and an improved understanding of the processes generating those changes. We report short-term (2014–2022) transformations of the proglacial landscape in front of Kviárjökull, SE Iceland, and place them in a longer-term context of glacial landsystem evolution using aerial image archives since 1945. Short-term quantification uses a time series of uncrewed aerial vehicle (UAV) surveys, processed utilizing a structure-from-motion (SfM) workflow, to produce digital elevation models (DEMs) and orthophoto mosaics. The land elements surveyed include a kame terrace staircase, an outwash plain, an ice-cored hummocky moraine complex and ice-cored hummocky terrain with discontinuous sinuous ridges, for which elevation and volumetric changes are quantified. The kame terraces between 2014 and 2022 and the outwash plain between 2016 and 2022 were mainly stable with, respectively, 87% and 85% of their surfaces showing no change. The ice-cored hummocky terrain with discontinuous sinuous ridges underwent a volume loss of 64,632 m^3 in 2016–2022, with a maximum surface lowering of ≤9 m. The most dynamic land element was the ice-cored hummocky moraine complex, with transformations recorded for more than 87% of its area in 2014–2022; the surface was lowered by ≤23 m in some places, with a total volume loss of 365,773 m^3. Our results confirm the ongoing degradation of ice-cored moraine and outwash complexes at variable rates related to buried ice volume and age of deglaciation. The evolution of chaotic hummocky terrain from debris-covered glacier ice, glacitectonic thrust masses, outwash fans/heads and complex englacial esker networks is an important modern analogue for informing palaeoglaciological reconstructions.

KEYWORDS
change detection, debris-charged glacial landsystem, glacial geomorphology, proglacial landforms, UAV, uncrewed aerial vehicle

1 | INTRODUCTION

Global climate warming has contributed to landform transformation for decades (Song et al., 2018) and increasing average air temperatures have resulted in significant changes in regional climates and local ecosystems, thereby increasing the risks of fires, droughts, floods and landslides (Allen et al., 2010; Flannigan et al., 2009; Gariano & Guzzetti, 2016; Hirabayashi et al., 2013; Młynarczyk et al., 2022). In cold climate settings, the impact has been manifested as dynamic responses in glacial systems (Benn et al., 2012; Benn & Evans, 2010). The recent fluctuations in volume and extent of glaciers have been widely analysed (e.g., Bash et al., 2018; Bash & Moorman, 2020; Carrivick et al., 2019; Hugonnet et al., 2021; Jouvet et al., 2019; Kienholz et al., 2020; Małecki, 2016; Małecki, 2022; Rossini et al., 2018; Sziło & Bialik, 2018) but less attention has been paid to geomorphological transformations taking place in proglacial areas and their possible links to climate warming (Bennett et al., 2010; Bennett & Evans, 2012; Carrivick & Heckmann, 2017; Chandler, Chandler, et al., 2020; Evans et al., 2023; Ewertowski et al., 2019; Ewertowski & Tomczyk, 2020; Hedding et al., 2020; Schomacker, 2008; Seier et al., 2017; Staines et al., 2015; Strzelecki et al., 2018).

Observations on landscape change in proglacial areas are important because such terrains contain a large amount of often unstable, non-consolidated sediments as well as water stored in the form of lakes and ice-cored landforms. The combination of potentially large volumes of meltwater and highly mobile sediments means that rapid, climate-driven transformations in proglacial areas can release substantial, possibly catastrophic, floods and/or debris flows, which in turn can rapidly transform landscapes located downstream (Carrivick & Tweed, 2019; Knight & Harrison, 2012a, 2012b; Knight & Harrison, 2018; Tomczyk et al., 2020; Tonkin et al., 2016). In inhabited parts of mountain and polar regions, the dynamics and scale of landform transformations on glacial forelands may have serious implications for infrastructure and human populations located in the same catchment (Cook et al., 2016, 2018; Harrison et al., 2018). Therefore, there is a strong justification for the monitoring of proglacial areas in such settings in order to understand the temporal aspects of landscape change during deglaciation, especially the de-icing of buried glacier ice masses (Bennett & Evans, 2012; Blauvelt et al., 2020; Evans et al., 2023; Ewertowski & Tomczyk, 2015; Kjær & Krüger, 2001; Krüger & Kjær, 2000; Schomacker, 2008; Schomacker & Kjær, 2007, 2008), as they pertain to applied glacial and paraglacial geomorphology (Carrivick & Heckmann, 2017). Not unrelated to this is the need to better quantify glacial process–form regimes as they pertain to spatio-temporal change in modern glacial landsystems (e.g., Bennett et al., 2010; Bennett & Evans, 2012; Chandler, Chandler, et al., 2020; Evans et al., 2009, 2019, 2022; Evans & Twigg, 2002; Ewertowski et al., 2019; Eyles, 1983a, 1983b; Midgley et al., 2018; Price, 1980).

Most of the previous research on proglacial landscape transformations has focused on the analysis of changes in the glacier forelands on a decadal temporal scale (e.g., Bennett & Evans, 2012; Carrivick & Heckmann, 2017; Etzelmüller, 2000; Ewertowski, 2014, 2019; Staines & Carrivick, 2015). Recently, a number of studies have begun the quantification of changes that take place on shorter temporal scales, from years to days (e.g., Bernard et al., 2016; Bühler et al., 2016; Chandler, Evans, et al., 2020; Evans et al., 2023; Ewertowski & Tomczyk, 2015; 2020; Fey & Krainer, 2020; Groos et al., 2019; Jouvet et al., 2018; Kraaijenbrink et al., 2016; Rossini et al., 2018; Ryan et al., 2015; van der Sluijs et al., 2018; van Woerkom et al., 2019; Westoby et al., 2020), typically using mobile platforms and sensors to collect data (e.g., LIDAR or uncrewed aerial vehicle [UAV]; Śledź et al., 2021 for detailed review). Because of their more detailed temporal and spatial scale, these studies do not cover whole glacial forelands but instead only individual landforms or single landform assemblages.

The aim of this study is to illustrate and quantify the short-term evolution of several different glacial landform assemblages on the foreland of the temperate, debris-charged glacier Kviárjökull in Iceland based on time series of UAV images. This foreland is an exceptional example of a landscape produced by the process of incremental stagnation (sensu Bennett & Evans, 2012; Eyles, 1979), whereby belts of debris-charged ice, representative of periodic influxes of debris to the glacier system, arrive occasionally at the receding glacier snout and give rise to the production of inset sequences of ice-cored hummocky moraine arcs over time. Each hummocky moraine arc therefore records the detachment of a debris-charged portion of the snout that is covered with supraglacial debris, retarding normal ablation rates. During progressive but slow de-icing, the hummocky moraine is subject to proglacial pushing or bulldozing by the actively receding glacier margin (Bennett et al., 2010; Bennett & Evans, 2012). Also important on the foreland of Kviárjökull are landform assemblages representative of sedimentation and landform construction in a high debris turnover piedmont glacier terminating in an erosional overdeepening. This has given rise to the development of unusually large latero-frontal terminal moraines, inset with extensive ice-contact glacifluvial landform–sediment associations. These include kame terraces, englacial eskers and pitted outwash, all reflective of the large sediment loads of meltwater networks that have developed over the overdeepening and which have been confined proglacially by the enclosing latero-frontal moraine amphitheatre (Bennett et al., 2010; Bennett & Evans, 2012; Phillips et al., 2017; Spedding & Evans, 2002).

Previous quantification studies at Kviárjökull by Bennett and Evans (2012) provided details on landform change relating to the melt-out of buried glacier ice and concomitant collapse of the ice-cored hummocky moraine arcs. They also documented the impact of the 1990s readvance (sensu Bradwell et al., 2006; Evans & Chandler, 2018; Evans & Hiemstra, 2005; Sigurðsson, 2005; Sigurđsson et al., 2007) of the glacier snout into the innermost moraine arc, which resulted in a phase of landform surface uplift by an average of 6.5 m following on from decades of collapse due to de-icing. This study aims to provide a continuation of the quantification of Bennett and Evans (2012) in order to evaluate the rate and extent of landscape degradation representative of modern-day glacierized settings characterized by debris-charged snouts with strong topographical constraints and subject to rapid melting in a warming

climate. An additional aim here is to facilitate the development of glacial process–form models constrained by real-time quantification, thereby strengthening, and indeed improving, those traditionally developed largely by ergodic principles (i.e., location for time reasoning, whereby a spatio-temporal continuum of landform genesis is reconstructed using examples of the landform at various stages of its development regardless of location; cf. Brunsden & Thornes, 1979; Evans, 2013; Evans & Twigg, 2002; Paine, 1985; Price, 1969).

2 | MATERIALS AND METHODS

This study is focussed on landform assemblages located on the northern part of the foreland of Kviárjökull, a temperate, debris-charged outlet glacier of the Öræfajökull ice cap in SE Iceland (Figure 1a), and records their transformation based on time series of aerial photograph archives (Figure 1) and UAV data. Longer timescale change (decadal) was mapped using the digital scans of aerial photographs (0.5–0.9 m ground sampling distance [GSD], that is, ground distance between centres of two pixels) from National Land Survey of Iceland captured in 1945, 1964, 1980 and 1998 by Landmaelingar Islands and in 2003 by Loftmyndir ehf (see Bennett et al., 2010, for details) as well as pan-sharpened (0.5 m GSD) WorldView-2 satellite imagery from Maxar (formerly Digital Globe) for 2012 and 2014. For shorter timescales, we used the popular structure-from-motion (SfM) method (see Westoby et al., 2012) to produce digital elevation models (DEMs) and orthomosaics based on four sets of images obtained from different types of UAVs: fixed-winged (produced by SmartPlane) and several generations of Phantom series quadcopters (produced by DJI) (Table 1). Autonomous flights were carried out in 2021 (Phantom 4 Pro) and 2022 (Phantom 4 RTK), and partly in 2014 (Smartplane), while flights with Phantom 2 in 2014 and Phantom 3 in 2016 were conducted manually. PlanetScope satellite images (3 m GSD) (Planet, 2022), combined with our UAV orthomosaics, were used to map changes in the glacier front during our observation period of 2014–2022.

During the 2022 flying, the UAV was connected to a local GNSS base station in order to increase the accuracy of the coordinates of the images, facilitated by the use of a high-precision RTK survey. The Topcon Link and RTKLIB software were used for post-processing and the application of PPP corrections (Precise Point Positioning) for the 2022 set of images and Ground Control Points (GCPs), along with an estimation of the influence of ocean tides on the measurement (source: http://holt.oso.chalmers.se/loading/). The image sets were used to create DEMs and orthomosaics in the Agisoft Metashape 1.7.1 photogrammetry software. Due to the fact that the UAV was equipped with an RTK receiver in 2022, we used one of the image processing schemes proposed by Nota et al. (2022), whereby we co-aligned all sets of images with seven GCPs marked on the 2022 images. We did not use the coordinates of the images from the other sets (2014, 2016 and 2021) as references. The result of this procedure was one, co-aligned, large, sparse point cloud, which was then divided into four separate projects according to the year of survey (2014, 2016, 2021 and 2022), in which only the right images for a given year were processed further to generate dense point clouds. Then, we proceeded to the next steps of processing using the Metashape software, and their detailed description is contained in Śledź and Ewertowski (2022), from which we chose the settings and parameters according to the procedure in script no. 2 'Optimal'. The only modification in the script was the higher accuracy of generating a sparse point cloud (from low to high) due to the partial use of JPG images and unsatisfactory results at the low level. Śledź and Ewertowski (2022) also describe and illustrate the method for establishing GCPs in the field, in the form of stone circles and the technique for measuring them with a GNSS receiver, which was identical in this study. The results of the photogrammetric processing were four DEMs, with the GSD ranging from 5.35 to 7.36 cm. Additionally, four high-resolution orthomosaics with GSD of ~3 cm were also exported.

Based on the DEMs and orthomosaics, we defined four case study areas on the glacier foreland which represent land elements (the fundamental level of the glacial landsystems hierarchy; sensu Eyles, 1983a, 2003; Fookes et al., 1978) within the debris-charged, active temperate glacial landsystem at Kviárjökull (Bennett et al., 2010) (Figure 2). These areas differ from each other in terms of their genesis, material properties and morphology, as well as the rate and scale of surface changes. To estimate changes on the foreland in a quantitative way, we used DEMs of differences (DoDs; Wheaton et al., 2010), which are models showing elevation changes between two surveys. DoDs were calculated in ArcMap 10.8.1 using a Geomorphic Change Detection (GCD) add-in dedicated to this software (Source: http://gcd.riverscapes.xyz). Before importing the DEMs to the GCD, we resampled them down to 6 cm per pixel. We also performed an error analysis, whereby variations in elevation differences for the stable areas on each pair of DEMs were calculated to determine the minimum level of detection (minLoD) equalled to 0.2 m. The mapping of the studied area was based on orthomosaics, field surveys and photographic documentation.

3 | RESULTS

3.1 | Characteristics of land elements of the debris-charged, active temperate foreland at Kviárjökull

Four land elements characteristic of the foreland were selected to investigate recent surface change or transformations (Figure 3), including case study areas: (1) a kame terrace staircase; (2) an outwash plain; (3) an ice-cored hummocky moraine complex and (4) ice-cored hummocky terrain with discontinuous sinuous ridges. These are representative of the broader proglacial area/foreland as previously mapped by Bennett et al. (2010) and are characterized by different topographies and buried glacier ice content, in addition to their distinctive genetic origins based on observations since the earliest aerial photographs captured in 1945 (Bennett et al., 2010; Bennett & Evans, 2012; Eyles, 1979, 1983b; Spedding & Evans, 2002).

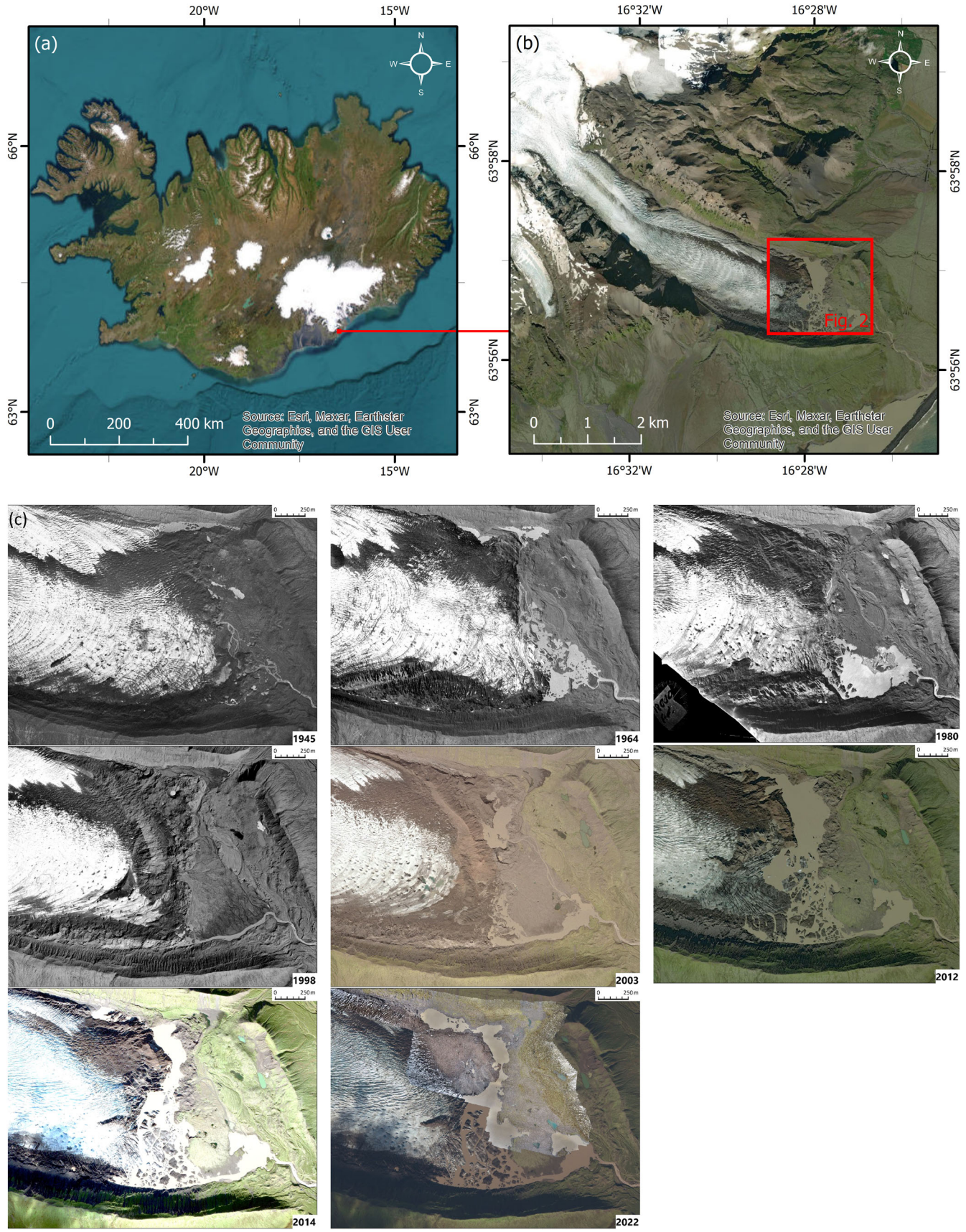

FIGURE 1 Kviárjökull, SE Vatnajökull, Iceland: (a, b) location of the study area; (c) aerial photograph (1945–2003) and satellite image (2012–2022) extracts from various times since 1945, showing the changes to the glacier snout and foreland. *Source*: 1945–2003—aerial photographs, National Land Survey of Iceland; 2012 and 2014—WorldView-2 images, Maxar (formerly Digital Globe); 2022—PlanetScope, Planet (2022). [Colour figure can be viewed at wileyonlinelibrary.com]

TABLE 1 Platforms used for quantifying recent, short timescale landscape change and the characteristics of the images.

Date	Drone	Total number of images	Images format	Type of sensor
2014, September	DJI Phantom 2 Vision+	38	DNG	Build-in, RGB
	Smartplane	347	JPG	Canon PowerShot S100, RGB
2016, September	DJI Phantom 3 Advanced	488	DNG	Build-in, RGB
2021, September	DJI Phantom 4 Pro	717	DNG	Build-in, RGB
2022, May	DJI Phantom 4 RTK	880	JPG	Build-in, RGB

Note: In 2014, two types of UAVs were used: a multi-rotor (DJI) and a fixed wing (Smartplane). Images from the fixed-wing and the DJI Phantom 4 RTK were saved in JPG format because these models do not allow saving in RAW format.

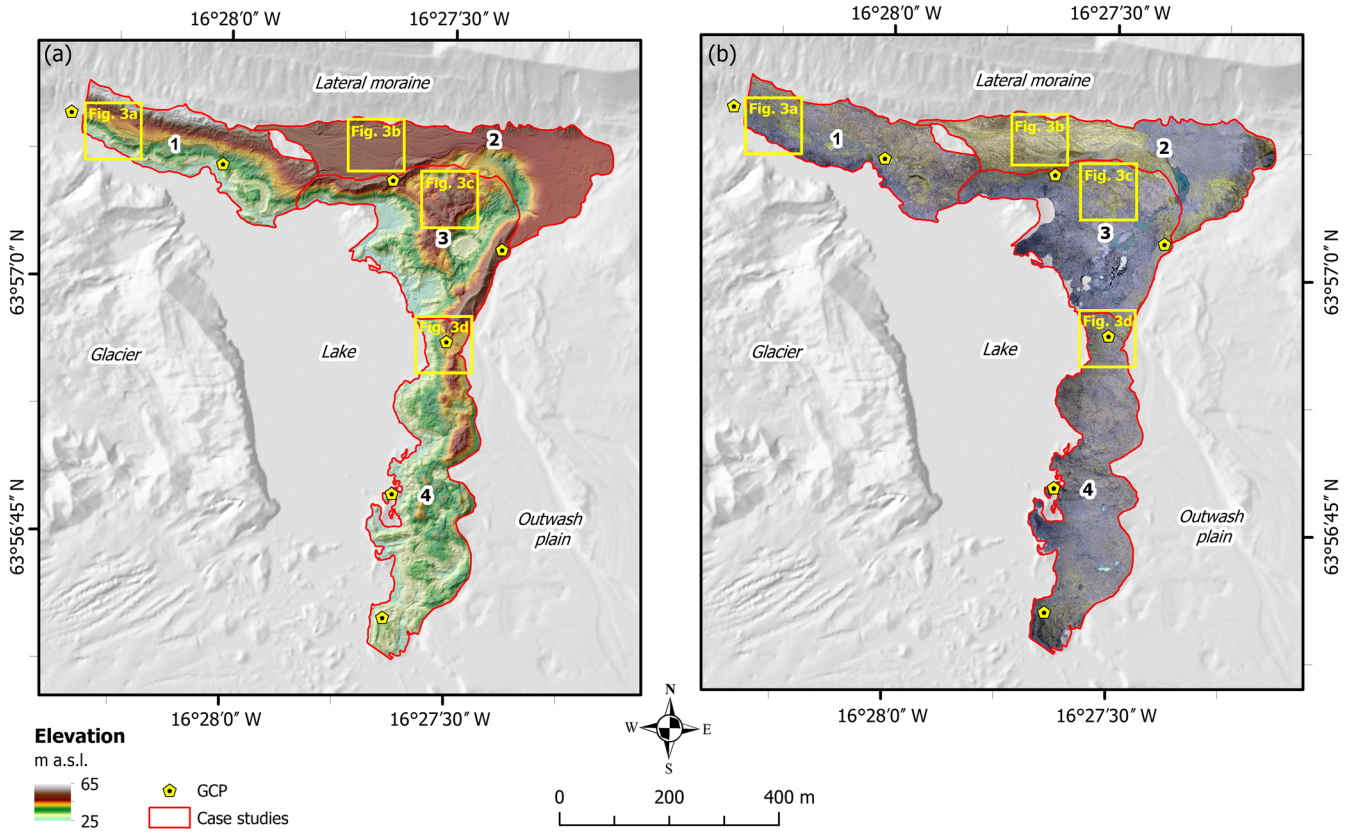

FIGURE 2 The extent of the four case study areas on the foreland of Kviárjökull (1: a kame terrace staircase; 2: an outwash plain; 3: an ice-cored hummocky moraine complex; and 4: ice-cored hummocky terrain with discontinuous sinuous ridges), with locations of Ground Control Points (GCPs) marked on the digital elevation model with hillshade (a) and orthomosaic (b) from September 2021. The figure also shows the location of the examples of the land elements in Figure 3. Source of background: ÍslandsDEM v1.0. *Source*: https://www.lmi.is/. [Colour figure can be viewed at wileyonlinelibrary.com]

The kame terrace staircase (case study area 1; Figures 2 and 3a) was developed between the ice margin and the steep proximal slope of the 100-m-high left lateral moraine (Kumbsmýrarkambur) on the foreland. Five to six distinct terrace levels were visible and characterized by tread widths of 8–25 m and riser heights of 4–13 m, the latter likely representing different period lengths of ice surface stabilization. Kame terraces are formed by meltwater flowing between the ice margin and any constraining slope, in this case the Kumbsmýrarkambur lateral moraine, so that each tread represents a former river bed that became abandoned once the glacier margin receded from the ice-contact slope/riser. Ground observations at the glacier margin since 1992 record the localized plunging of the meltwater streams beneath the glacier margin to form margin-parallel englacial tunnels whose glacifluvial infill are gradually buried by the aggradation of the terrace deposits (Figure 4); this results in the localized burying of remnant ice masses within the terraces (Bennett & Evans, 2012). The gradual melt-out of such buried ice masses gives rise to collapse pits, usually forming a hummocky/pitted appearance to the ice-contact slopes/risers. Additionally, the edges of some of the terrace treads are characterized by the superimposition of small (1–2 m high) push moraines,

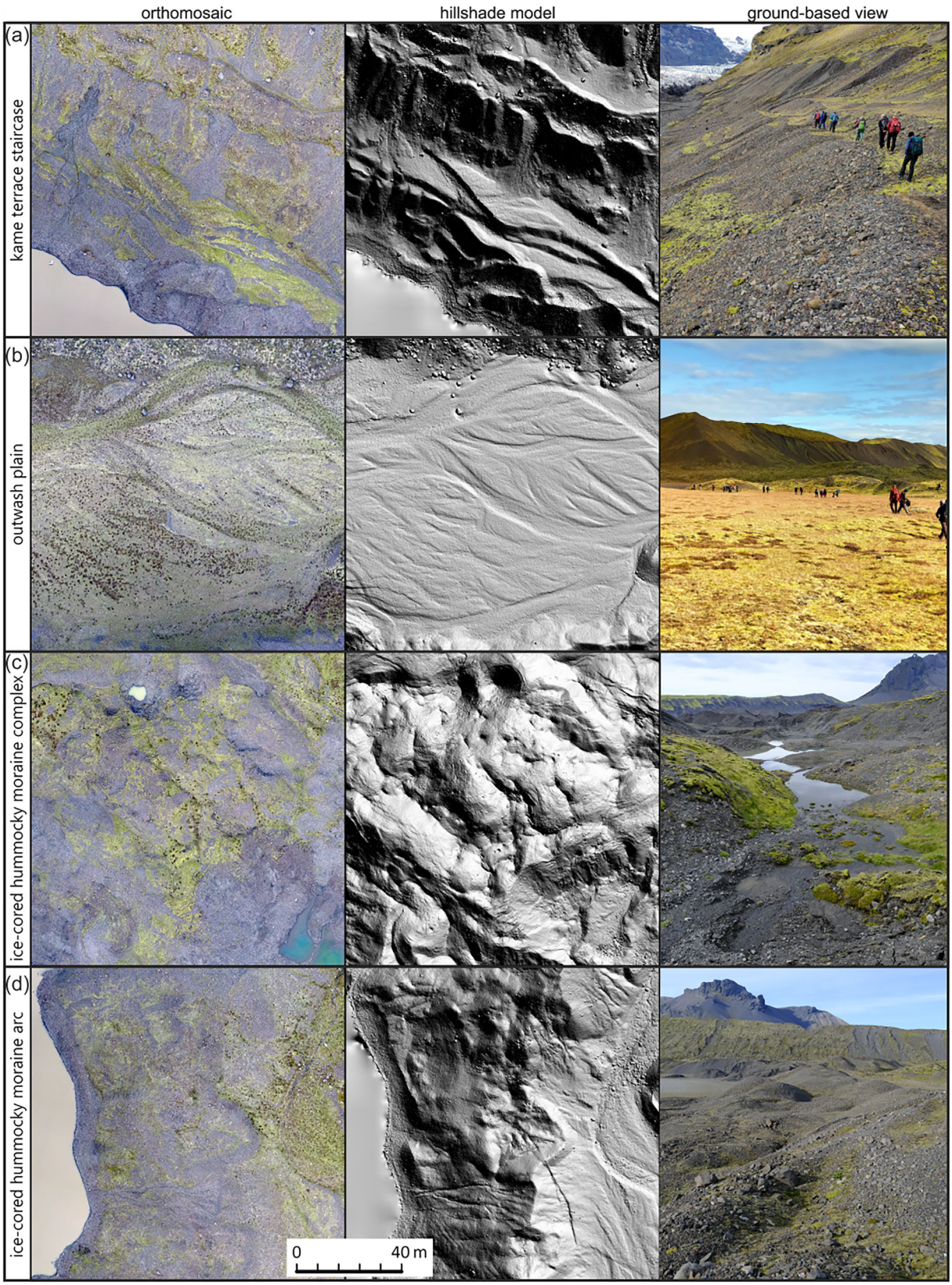

FIGURE 3 Examples of the landsystem elements on the foreland at Kviárjökull viewed using remotely sensing data and ground photographs: (a) kame terrace staircase; (b) outwash plain; (c) ice-cored hummocky moraine complex and (d) ice-cored hummocky terrain with discontinuous sinuous ridges—see Figure 2 for location. Note that all images in the columns 'orthomosaic' and 'hillshade model' are presented at the same spatial scale. [Colour figure can be viewed at wileyonlinelibrary.com]

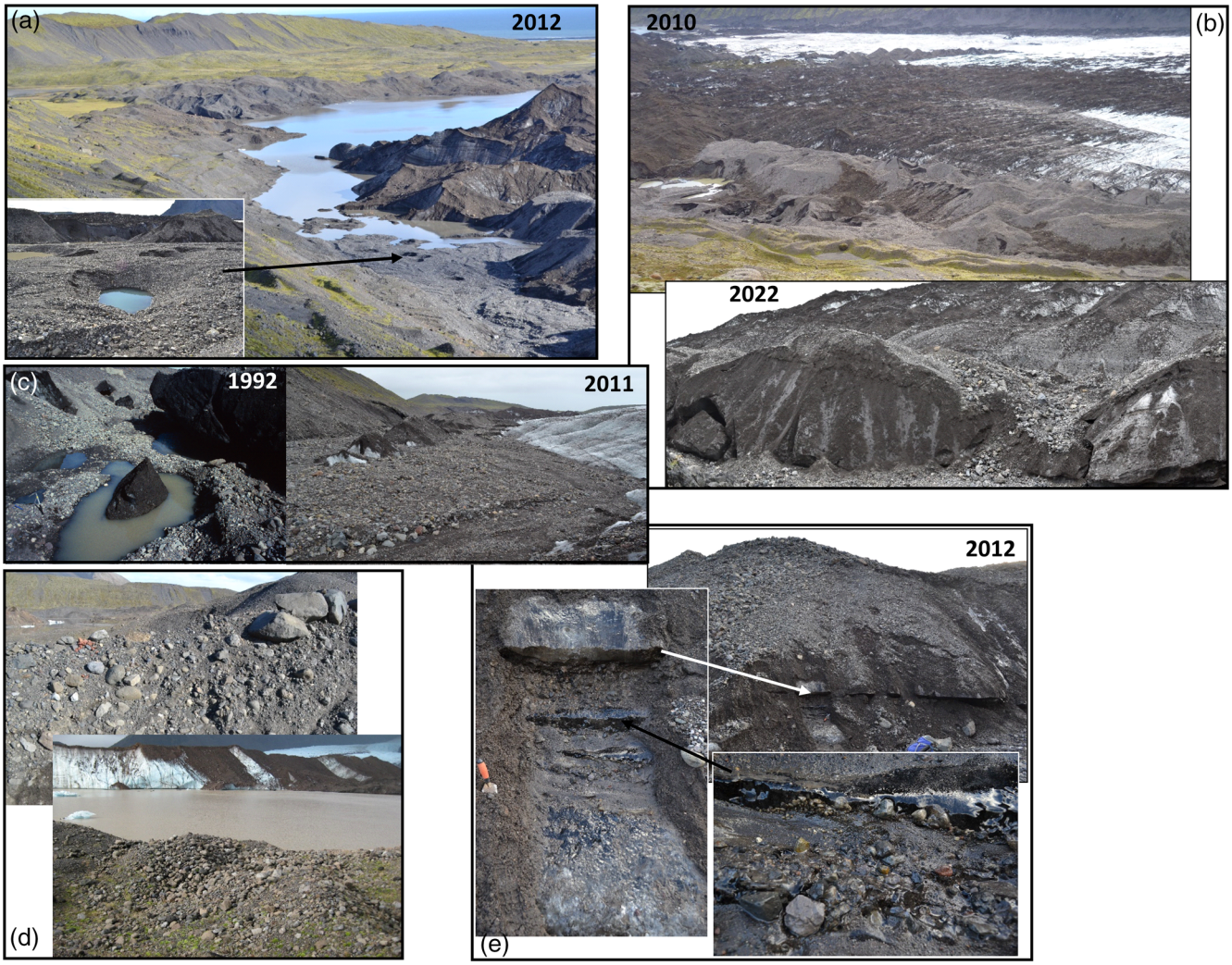

FIGURE 4 Field photographs of examples of the development of ice-marginal drainage and landform development along the northern margin of the snout captured at various times since 1992: (a) freshly abandoned pitted kame terrace in 2012, with active channel emerging from the ice below an englacial esker; (b) the englacial esker emerging in 2010 (grey-coloured gravel) and overlying ice with active tunnels, depicted in 2022 at a more advanced stage of collapse when the sub-marginal stream had abandoned the adjacent kame terrace; (c) remnant ice in the 1992 and 2011 kame terraces, emerging through marginal outwash gravel and representing collapsed and buried tunnels originally cut by sub-marginal streams; (d) mounds of water-worn gravels forming parts of the sinuous ridges emerging within the ice-cored hummocky moraine during downwasting due to melt-out in 2008 and (e) cross-sections through sub-marginal/englacial tunnel fills exposed after stream downcutting in 2012. [Colour figure can be viewed at wileyonlinelibrary.com]

some of which have been observed during formation (Phillips et al., 2017; Figure 3a). Continuous paraglacial reworking of the lateral moraine and the kame terraces has resulted in widespread dissection by debris flow and fluvial channels as well as the deposition of small debris flow-fed lobes and fans.

The outwash plain (case study area 2; Figures 2 and 3b) is a continuation of the highest of the kame terraces and forms a down-valley widening fan that was deposited around and over the outer downwasting glacier snout in the 1980s–1990s, infilling a proglacial/supraglacial lake that occupied the area in the 1960s–1980s (Bennett et al., 2010; Figure 1c). The meltwater deposited a large (~32,800 m^2), flat area of glacifluvial sediments, overlying lake deposits and located between the ice-cored hummocky moraine complex and the former position of the 1990s ice margin to the south and the Kumbsmýrarkambur lateral moraine to the north. The 1990s readvance moraine (sensu Bradwell et al., 2006; Evans & Chandler, 2018; Evans & Hiemstra, 2005; Sigurðsson, 2005; Sigurðsson et al., 2007) was constructed on the ice-contact face of the fan and now forms a prominent ridge along part of its southern edge. A network of braided stream channels is clearly visible on the outwash plain surface (Figure 3b) and small alluvial and debris flow-fed fans and isolated boulders have been deposited on its northern edge by paraglacial processes operating on the steep slopes of the Kumbsmýrarkambur lateral moraine.

The ice-cored hummocky moraine complex (case study area 3; Figures 2 and 3c) is a triangular-shaped area approximately 300 m long and up to 350 m wide, characterized by a chaotic hummocky topography with numerous, continuously expanding and contracting

areas of exposed glacier ice as a result of rapid and widespread topographic reversal (moraine belt A of Bennett & Evans, 2012). The outermost ridges of the complex are the product of pushing of the buried, stagnant ice mass into the outwash plain to the north and east as a result of the 1990s readvance, during which the surface of the ice-cored hummocky moraine belt increased in elevation by an average of 6.5 m (Bennett et al., 2010; Bennett & Evans, 2012). As a result, the easternmost edge of the moraine complex is very steep and separated from another, older hummocky moraine belt (hummocky moraine complex B of Bennett & Evans, 2012) by a narrow linear sandur that became constricted by the encroachment of the outer moraine edge and was then abandoned by meltwater drainage in the late 1990s (Figure 1c). These inset hummocky belts are the landform signature of incremental stagnation, with the overprinting of push ridges and/or development of glacitectonic structures that document readvance events such as the 1990s readvance (Bennett & Evans, 2012). Since around 2000, a proglacial and partially supraglacial lake (Figure 2) has developed at the western margin of the hummocky moraine complex as a result of more rapid ablation of the sparsely debris-covered glacier snout located up-ice. Lake development is a consequence of the gradual uncovering of the ≤100-m-deep overdeepening beneath the snout in this area (Spedding & Evans, 2002). In 2014, the highest hummocks reached 25 m above the water level, but as the degradation intensified, the maximum elevation above the lake was only 15 m in 2022. Sediments that have been visible in the outcrops created by topographic inversion over the last 20 years have ranged from poorly sorted boulder to cobble gravels, gravelly diamictons and localized pockets of well-sorted stratified gravels and sands, the latter representing the melt-out of englacial tunnels/eskers (Bennett et al., 2010; Bennett & Evans, 2012; Spedding & Evans, 2002). Numerous tension cracks, freshly developed collapse pits/sink holes, damp surface sediment and debris flows are visible on the hummocky moraine surface and indicate the presence and ongoing degradation of buried glacier ice (Figure 3c).

Case study area 4 (Figures 2 and 3d) is a 650-m-long arc of ice-cored hummocky terrain with discontinuous sinuous ridges that extends southwards from the ice-cored hummocky moraine of case study area 3. It forms the hummocky ice-proximal face of the large pitted outwash plain previously interpreted by Bennett and Evans (2012) as an emerging outwash head occupying the adverse slope of the underlying bedrock overdeepening. The width of the moraine belt varies from 70 to 200 m with elevations reaching 10–15 m above the proglacial/supraglacial lake level in 2016. Like the hummocky moraine to the north, the hummocks and ridges in case study area 4 comprise a range of poorly sorted boulder to cobble gravels, gravelly diamictons and well-sorted stratified gravels and sands, with the latter clearly relating to west–east trending sinuous ridges that have developed since the 1990s due to the melt-out of englacial eskers linked to the apex of the outwash head (Bennett et al., 2010; Bennett & Evans, 2012; Spedding & Evans, 2002). The outermost ridges of the ice-cored hummocky terrain are arcuate to slightly sinuous in plan form but orientated ice-margin parallel and are push moraines constructed in ice-proximal outwash during the 1990s readvance.

3.2 | Glacier snout changes

Between 2011 and 2022, the ice margin was highly dynamic and oscillatory and additionally there was a significant difference in the behaviour between the northern and southern parts of the snout (Figure 5). The margin in the southern part of the snout underwent an almost continuous and gradual retreat (except for 2018, when it advanced by ~120 m) as the glacier downwasted and disintegrated through the formation of widening crevasses and their flooding to produce tabular icebergs on the expanding proglacial/supraglacial lake. The northern part of the snout advanced by ~200 m in the period 2013–2018 and then remained stable from 2019 to 2022. Likely influential in this varied response is the fact that the southern and northern margins of the snout are fed by different ice-flow units, which flow down either side of a nunatak in the accumulation zone and are nourished in source basins of different sizes. Additionally, ablation rates and hence the extent of glacier surface downwasting will vary significantly between the two ice-flow units in the snout zone (Figure 1c). The southern part of the glacier is characterized by large areas of debris-poor ice and, with the exception of the supraglacial lateral moraines and arcuate debris bands on the extreme southern margin, lacks a supraglacial debris cover. In contrast, the northern part of the glacier has always been characterized by an extensive debris cover delivered to the snout by the pulsed delivery of englacial and supraglacial debris which results in the retardation of ablation (incremental stagnation; Bennett & Evans, 2012). Moreover, the two ice-flow units have different dynamics, whereby the north ice-flow unit has exhibited some significant readvances in addition to that of the 1990s (Phillips et al., 2017). Also, likely important is the apparent glacier karst network, manifested as numerous moulins, which has remained a stable characteristic of the southern ice-flow unit over time and indicates that a complex englacial-to-subglacial tunnel network exists and results in substantial ice surface collapse during down wasting. All of these characteristics are exacerbated by the continuously rapid growth of the proglacial/supraglacial lake since 2011.

3.3 | Recent transformations of the land elements

Using the DoDs, land surface and volume change are now presented for the four case study areas (land elements) over the last 8 years or less. Due to differences in the temporal coverage of aerial imagery, the first year of analysis is either 2014 or 2016. Areal, volumetric and vertical averages calculated from DoDs for each land element are summarized in Table 2.

3.3.1 | Case study area 1 (kame terraces)

Between 2014 and 2022, most of the kame terrace staircase was stable (Figure 6a) and detectable changes occurred in only 14% of the area, with a total net volume difference of −6402 ± 1118 m^3, reaching an average net thickness change of −0.99 ± 0.17 m (Table 2). A

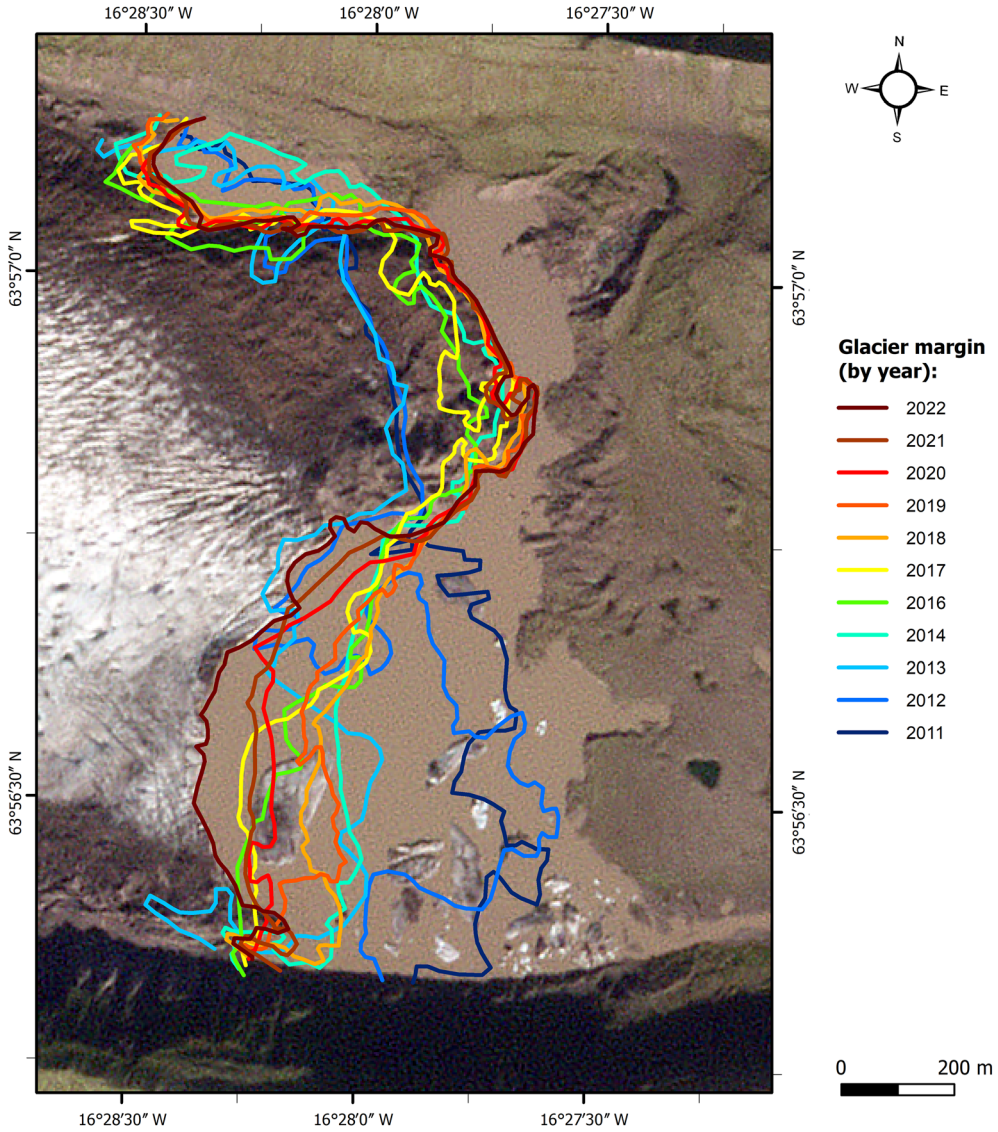

FIGURE 5 Changes in the margin of the glacier snout in the period 2011–2022 based on the PlanetScope satellite imagery (Planet, 2022). Note that in 2015, scenes from PlanetScope were not available for this location. Date of the background image is 2022. [Colour figure can be viewed at wileyonlinelibrary.com]

decrease in elevation of up to 10 m was recorded for the southern fringe (Figure 6a) or the most recent kame terraces, which was related to melting of the residual buried glacier ice that was created where marginal streams plunged into the lateral margin of the glacier and continued over short distances in englacial tunnels (Figure 4). An increase in elevation of up to 1 m was observed in the upper parts of the terrace sequence, which is likely associated with transfer of sediments from the adjacent lateral moraine slopes by mass movements. A further small area of positive change (≤3 m) occurred in the south-east tip of the most recent terraces and is associated with push moraine construction on their former ice-contact slopes during the 2014 snout readvance (Phillips et al., 2017).

3.3.2 | Case study area 2 (outwash plain)

Large areas of the outwash plain (Figures 2 and 7) also remained partly stable over the last 6 years. The changes in the period 2016–2022 took place on only ~15% of the surface, with a total net volume difference of 15,440 ± 1764 m^3 (Figure 7c, Table 2). Two significantly active areas occur in the eastern half of the outwash plain. Firstly, an arcuate, lake-filled collapse pit occurs at the boundary of the ice-cored hummocky moraine complex (see case study area 3; Figure 7c), where the highest values of elevation loss of >3 m are recorded. The degradation of buried ice here started with the development of small, dry sink holes, which enlarged until the buried ice became visible and the expansion of sink holes led to the development of chains of depressions and, finally, to the formation of a single, large elongate depression. This depression has gradually extended northwards to the foot of the Kumbsmýrarkambur lateral moraine slope and is surrounded by arcuate concentric tension fault scarps. The western edge of the depression is dissected by a 25-m-long, ≤3-m-deep erosion gully (Figure 7e), which started developing after 2014. The increase in elevation between 2021 and 2022 (Figure 7b) is related to fluctuations in water level, which filled up the depression created between 2014 and 2021. Second, at the eastern, distal extremity of the

TABLE 2 Areal, volumetric and vertical change averages derived from DEMs of differences for each case study.

DoD	Total area of surface lowering (m^2)	Total area of surface raising (m^2)	Total area of detectable change (m^2)	Pre cent of area of interest with detectable change (%)	Total volume of surface lowering (m^3)	Total volume of surface raising (m^3)	Total net volume change (m^3)	Average depth of surface lowering (m)	Average depth of surface raising (m)	Average net thickness of difference (m) for area with detectable change
Case study 1 (kame terrace staircase)										
September 2014–September 2021	5676.20	1121.85	6798.05	14.15	7550.45 ± 1135.24	1019.99 ± 224.37	−6530.46 ± 1157.20	1.33 ± 0.20	0.91 ± 0.20	−0.96 ± 0.17
September 2021–May 2022	323.02	396.49	719.52	1.50	122.22 ± 64.61	92.58 ± 79.30	−29.64 ± 102.28	0.38 ± 0.20	0.23 ± 0.20	−0.04 ± 0.14
September 2014–May 2022	5502.00	982.57	6484.57	13.49	7344.58 ± 1100.40	942.95 ± 196.51	−6401.62 ± 1117.81	1.33 ± 0.20	0.96 ± 0.20	−0.99 ± 0.17
Case study 2 (outwash plain)										
September 2016–September 2021	9074.76	412.60	9487.36	15.36	15,792.40 ± 1814.95	141.78 ± 82.52	−15,650.61 ± 1816.83	1.74 ± 0.20	0.34 ± 0.20	−1.65 ± 0.19
September 2021–May 2022	210.33	865.61	1075.94	1.74	75.18 ± 42.07	267.95 ± 173.12	192.76 ± 178.16	0.36 ± 0.20	0.31 ± 0.20	0.18 ± 0.17
September 2016–May 2022	8811.90	409.10	9221.00	14.94	15,582.33 ± 1762.38	142.13 ± 81.82	−15,440.21 ± 1764.28	1.77 ± 0.20	0.35 ± 0.20	−1.67 ± 0.19
Case study 3 (ice-cored hummocky moraine complex)										
September 2014–September 2016	54,685.07	748.31	55,433.38	83.49	90,448.73 ± 10937.01	265.07 ± 149.66	−90,183.66 ± 10938.04	1.65 ± 0.20	0.35 ± 0.20	−1.63 ± 0.20
September 2016–September 2021	55,483.78	425.78	55,909.56	84.21	256,699.33 ± 11096.76	203.27 ± 85.16	−256,496.07 ± 11097.08	4.63 ± 0.20	0.48 ± 0.20	−4.59 ± 0.20
September 2021–May 2022	17,276.40	1440.67	18,717.06	28.20	17,720.79 ± 3455.28	513.23 ± 288.13	−17,207.55 ± 3467.27	1.03 ± 0.20	0.36 ± 0.20	−0.92 ± 0.19
September 2014–May 2022	57,304.12	753.32	58,057.43	87.41	366,080.27 ± 11460.82	307.27 ± 150.66	−365,773.00 ± 11461.81	6.39 ± 0.20	0.41 ± 0.20	−6.30 ± 0.20
Case study 4 (ice-cored hummocky terrain with discontinuous sinuous ridge)										
September 2016–September 2021	42,688.40	266.32	42,954.72	60.14	60,392.62 ± 8537.68	64.32 ± 53.26	−60,328.30 ± 8537.85	1.41 ± 0.20	0.24 ± 0.20	−1.40 ± 0.20
September 2021–May 2022	5828.46	170.91	5999.38	8.40	1908.44 ± 1165.69	56.66 ± 34.18	−1851.78 ± 1166.19	0.33 ± 0.20	0.33 ± 0.20	−0.31 ± 0.19
September 2016–May 2022	43,336.43	427.42	43,763.85	61.26	64,733.01 ± 8667.29	101.43 ± 85.48	−64,631.58 ± 8667.71	1.49 ± 0.20	0.24 ± 0.20	−1.48 ± 0.20

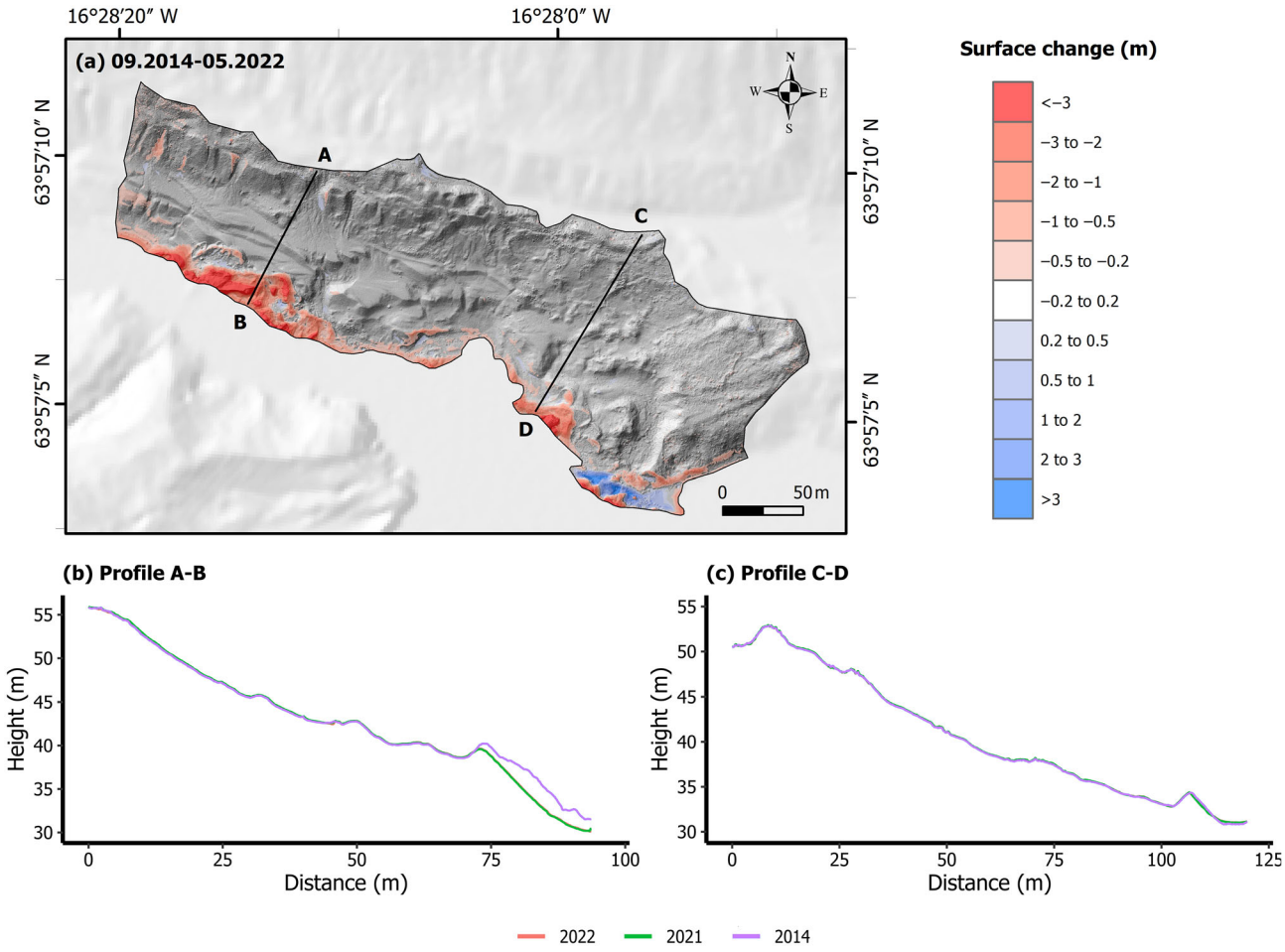

FIGURE 6 Elevation changes for the kame terrace staircase (case study area 1—see Figure 2 for location) between 2014 and 2022. The minLoD was set at 0.20 m. Source of background: ÍslandsDEM v1.0. [Colour figure can be viewed at wileyonlinelibrary.com]

outwash plain, a large, shallow collapse pit records the sinking of the outwash surface by up to 0.5 m. Other minor recorded changes include deposition in the north-eastern corner of the outwash plain where alluvial fans, debris flow-fed fans and boulders have accumulated as a result of paraglacial reworking of the steep slope of the Kumbsmýrarkambur lateral moraine.

3.3.3 | Case study area 3 (ice-cored hummocky moraine complex)

Case study area 3 is the area that underwent the most changes and maximum activity. Comparing 2014 with 2022 (Figure 8d), changes occurred in 87% of the case study area, reducing its volume by −365,773 ± 11,462 m^3 (Table 2). Maximum elevation changes during this 8-year period reached >20 m (Figure 8f). Importantly, the ice-cored moraine complex also shows significant changes in surface morphology within 1 year (Figure 8c—DoD 2021–2022), where the maximum recorded decrease in elevation was 8 m. The average net thickness of difference for DoD 2014–2022 was −6.30 ± 0.20 m, which demonstrates the dynamism of the degrading ice-cored complex, suggesting that further degradation should be expected. This high level of transformation was related to the melting and degradation of ice cores. The surface collapsed in several places, while indicators of downwasting, such as tension cracks and holes, are widespread. There is a fairly visible trend in the spatial distribution of highly active parts of the ice-cored moraine complex, with the highest rates of terrain collapse along the SW–NE axis, where a line of irregular, water-filled depressions was formed after 2016 (Figure 9). Another type of transformation was recorded along the lake shore, where the water edge enhanced debris sliding along the exposed ice cliffs, thereby facilitating ice melting. The inner part of the moraine complex was less dynamic, the transformations manifesting themselves through tension cracks and uneven lowering of different parts of the moraine.

3.3.4 | Case study area 4 (ice-cored hummocky terrain with discontinuous sinuous ridges)

The ice-cored hummocky terrain with discontinuous sinuous ridges also turned out to be active (Figure 10) as 61% of its area changed (Figure 10c—DoD 2016–2022) and its volume decreased by 64,632 ± 8668 m^3 (Table 2) over the course of 6 years. The average net

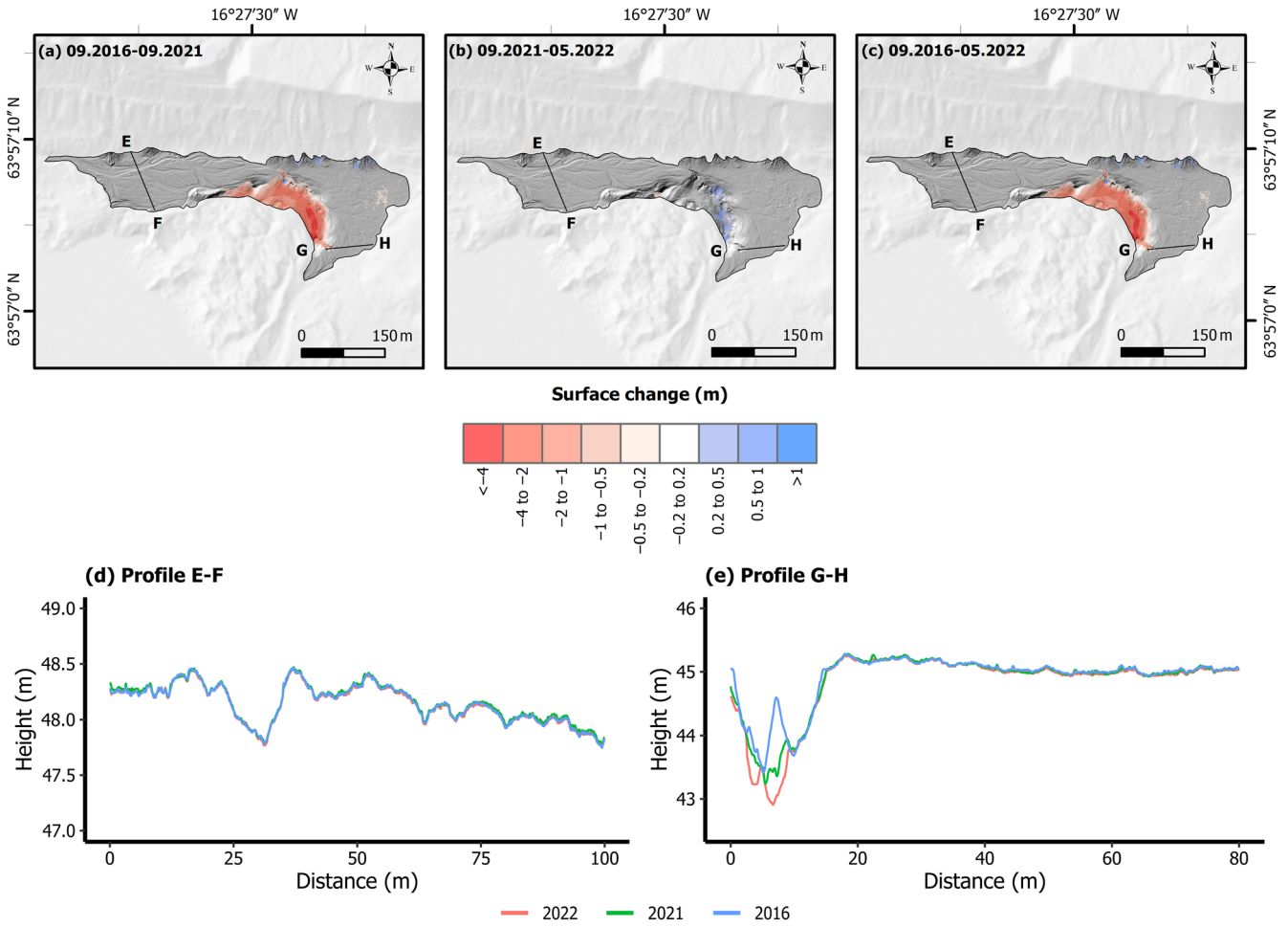

FIGURE 7 Elevation changes between 2016 and 2022 for the outwash plain (case study area 2—see Figure 2 for location). The minLoD was set at 0.20 m. Source of background: ÍslandsDEM v1.0. [Colour figure can be viewed at wileyonlinelibrary.com]

thickness of difference for the same DoD was −1.48 ± 0.20 m, but the highest decrease in elevation was >9 m. In the southern part of the area, minor surface accumulation was recorded, but no indicators of deposition were found during the field verification and so we treated this as an artefact due to an erroneous surface reconstruction for 2016. In the calculations for 2021–2022 (Figure 10b), a change in volume of −1852 ± 1166 m^3 was noted. Reflecting this, the M-N and O-P cross profiles (Figure 10d,e) in the central, most active part of the moraine clearly show that the changes in morphology are concentrated near the lake and along the central axis of the ridge, whereas the rest of the area is more stable.

4 | DISCUSSION

4.1 | Spatial and temporal distribution of surface changes

During the observation period (2014–2022), the study areas underwent various scales of change (Figures 6–10). Very little activity took place in case study areas 1 and 2, the kame terraces and outwash plain, where ~85% of the total surface had not changed in the period 2014–2022. In contrast, case study areas 3 and 4 underwent more dynamic activity, especially the ice-cored moraine of case study area 3, where only 13% of the surface remained stable over the same period (Table 2). Such a diverse response is directly related to the presence of dead ice and its melting. The average annual rate of change for 2021–2022 in all case study areas was lower than in other periods, likely because the survey period comprised mostly the winter season (September 2021–May 2022), before the beginning of the summer ablation peak.

4.2 | Processes responsible for surface changes

The degradation of buried dead ice blocks and associated mass movements, including ground surface collapse and widespread debris flows, were the most critical processes responsible for transformation of the ice-cored moraine complexes of study areas 3 and 4 over the period 2014–2022. This was evidenced by the

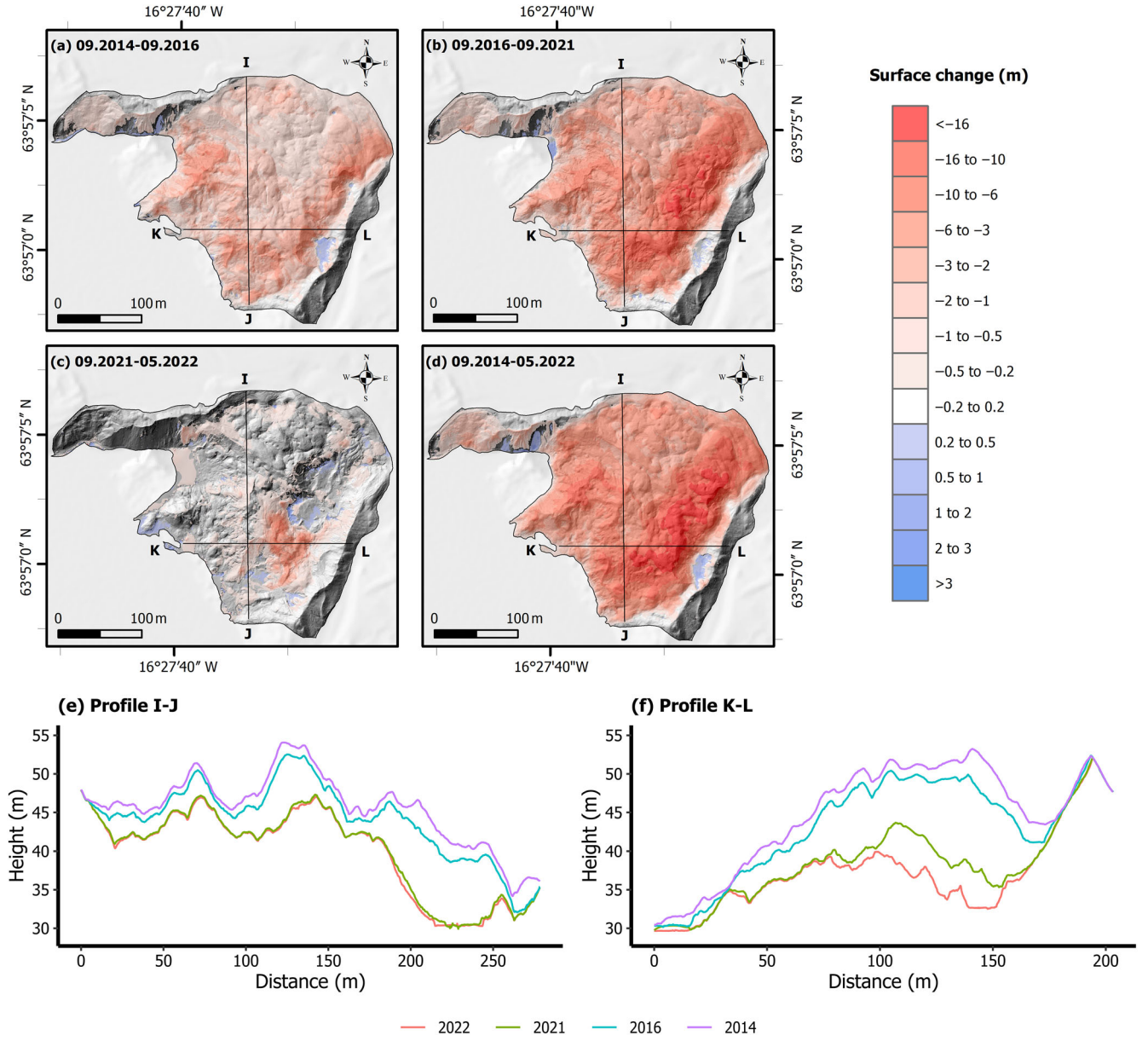

FIGURE 8 Elevation changes between 2014 and 2022 for the ice-cored hummocky moraine complex (case study 3—see Figure 2 for location). The minLoD was set at 0.20 m. Source of background: ÍslandsDEM v1.0. [Colour figure can be viewed at wileyonlinelibrary.com]

appearance and changing shape of numerous sinkholes and tension fractures on the moraine surfaces. Another process that impacted significantly on volume change was fluctuations in water levels and concomitant shore erosion around the margins of the proglacial/supraglacial lake and the ponds that developed in enlarging sink holes/kettles. Although surface collapse due to ice melt-out dominated as a process over the surveyed areas, some minor impacts and surface elevation increases were due to paraglacial activity in the historically developed and largely unstable lateral moraine topography, including the development of small debris flows, rockfalls, small rock avalanches and alluvial fans, which added debris to the tops of kame terraces and outwash margins.

4.3 | Comparison with short-term rates of surface change at other locations

To compare the land surface dynamics between case studies of varying areal extent, we standardized the volumetric measurements by dividing them according to area and period of observation, thereby ensuring that the average change in annual volume was calculated (Figure 11). The results confirm the low volumetric change of case study area 1 (average elevation changes of −0.13 m a^{-1}), the intermediate volumetric change of case study areas 2 and 4 (−0.29 and − 0.26 m a^{-1}, respectively, for the period 2016–2022) and the high-volume loss of case study area 3 (−0.82 m a^{-1} for the period 2014–2022). Additionally, Table 3 shows the maximum annual

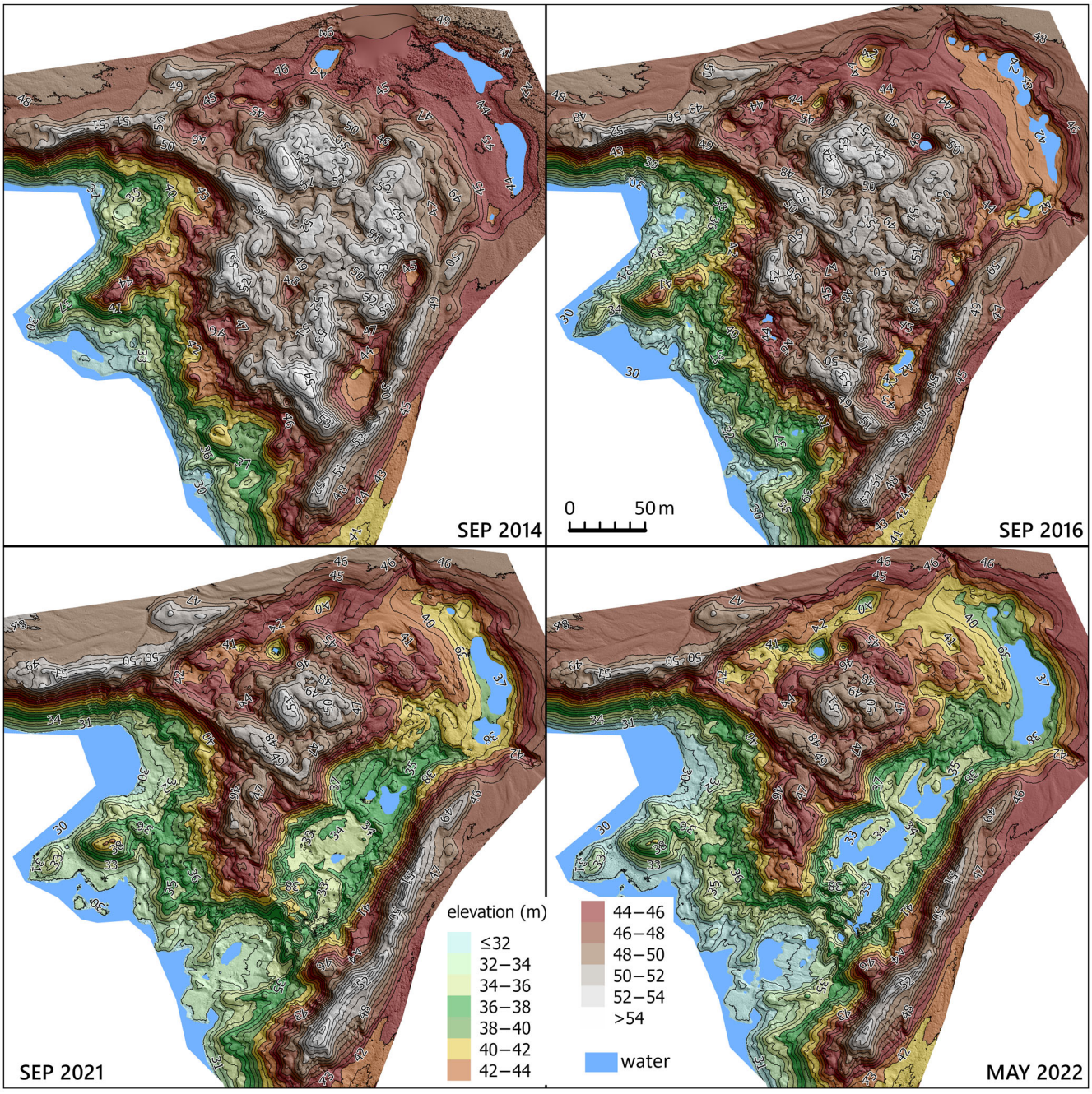

FIGURE 9 Evolution of ice-cored moraine complex at Kviárjökull between 2014 and 2022—see Figure 2 for location. [Colour figure can be viewed at wileyonlinelibrary.com]

thickness difference for each DoD calculation, ranging from −2 to −3 m a^{-1} for case study areas 1, 2 and 4 up to −12.21 m a^{-1} and for case study area 3 for 2021–2022.

This range of values for volumetric change due to de-icing on the contemporary foreland of a rapidly receding glacier can be compared with those in other settings (Table 4). For example, on the forelands of Ebbabreen and Ragnarbreen, Svalbard, the average annual changes in thickness (i.e., sum of elevation changes divided by the area and period of observation) for an ice-cored moraine complex from 2012 to 2014 ranged from −0.14 to −1.83 m a^{-1} and the average annual maximum thickness change (i.e., maximal values of elevation changes divided by the period of observations) ranged from −1.0 to −7.9 m a^{-1} (Ewertowski & Tomczyk, 2015). For the ice-cored moraine in the foreland of Midtre Lovénbreen, Svalbard, an average annual thickness change of −0.65 m a^{-1} was measured over the period 2003–2005 (Irvine-Fynn et al., 2011). For the same glacier, but a longer period (2003–2014), Midgley et al. (2018) reported changes ranged from −0.02 m a^{-1} for outwash plain (without buried ice) to −0.40 m a^{-1} for ice-cored medial moraine. In contrast, the ice-cored moraine on the neighbouring foreland of Austre Lovénbreen, Svalbard, displayed

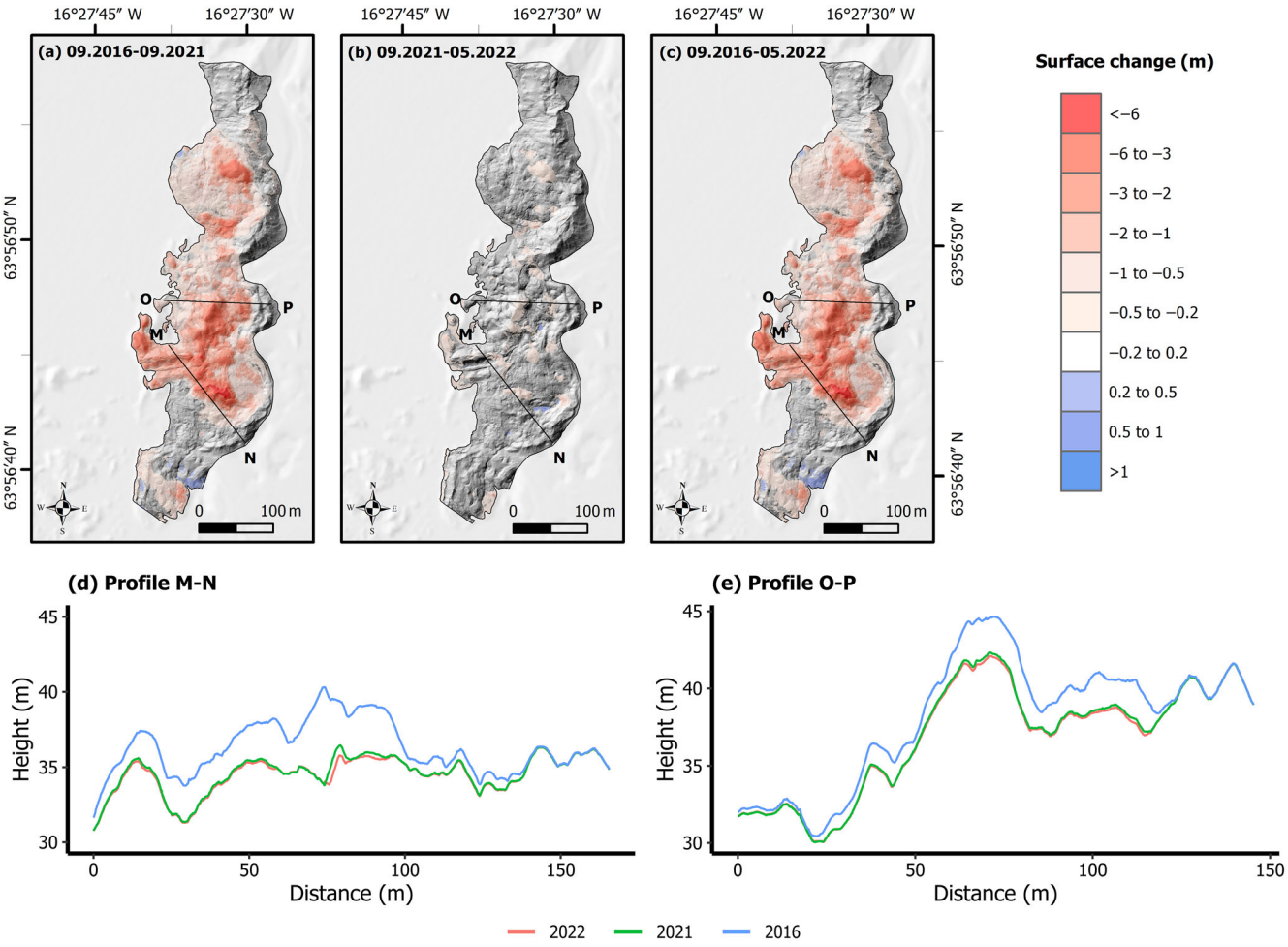

FIGURE 10 Elevation changes for the thrust ice-cored moraine arc (case study 4—see Figure 2 for location) for the years 2016–2022. The minLoD was set at 0.20 m. Source of background: ÍslandsDEM v1.0. [Colour figure can be viewed at wileyonlinelibrary.com]

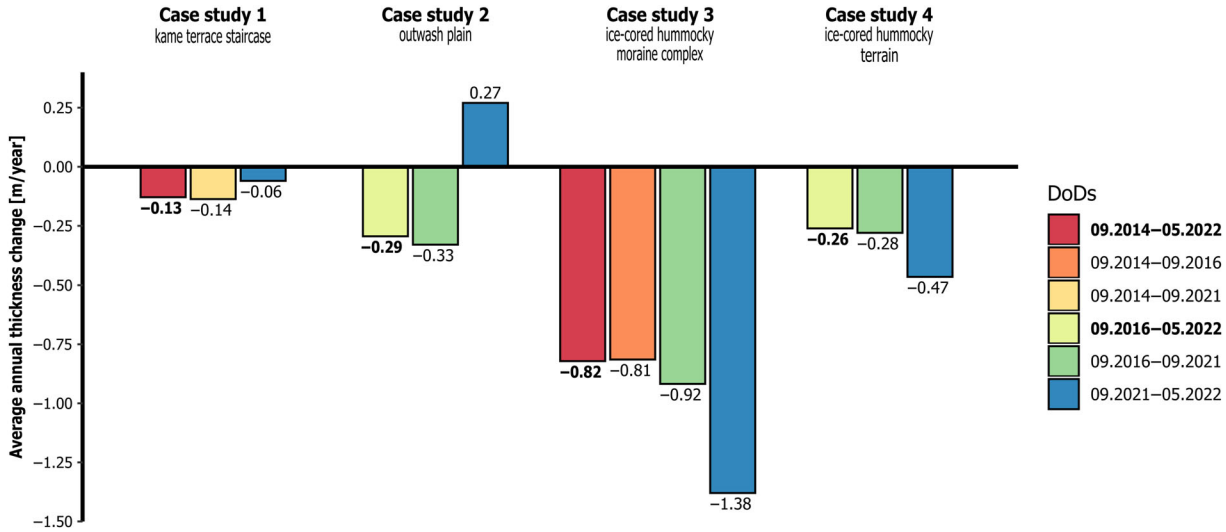

FIGURE 11 Average annual thickness change for different case study areas on the Kvíárjökull foreland. Changes calculated from the summary DoDs (i.e., differences between first and last surveys) for each case study area are indicated by bold fonts. [Colour figure can be viewed at wileyonlinelibrary.com]

TABLE 3 Average annual maximum thickness change for each case study area.

DoD	Average annual maximum thickness change (m)
Case study area 1	
September 2014–September 2021	−1.53
September 2021–May 2022	−2.70
September 2014–May 2022	−1.43
Case study area 2	
September 2016–September 2021	−1.26
September 2021–May 2022	−2.06
September 2016–May 2022	−1.02
Case study area 3	
September 2014–September 2016	−4.83
September 2016–September 2021	−3.81
September 2021–May 2022	−12.21
September 2014–May 2022	−2.96
Case study area 4	
September 2016–September 2021	−1.76
September 2021–May 2022	−2.69
September 2016–May 2022	−1.60

Note: Due to fact that the DoDs for September 2021–May 2022 are for a shorter period than 1 year, we calculate the mean with an accuracy of 1 month.

an average elevation change of only −1.42 m in the 11-year period 2003–2014 (~0.13 m a^{-1}), with the maximum change exceeding −4 m (Tonkin et al., 2016). Much greater change has been observed on the foreland of Fjallsjökull, Iceland, where calculations have been made on an annual basis between 2016 and 2019; from 2016 to 2017 in particular, the highest rate of average maximum elevation change of −0.5 m per month (6 m a^{-1}) was recorded (Chandler, Evans, et al., 2020). Other land elements in the foreland of Fjallsjökull and Hrútárjökull (Iceland) were characterized by average annual elevation changes between −0.08 and −1.33 m a^{-1} (Table 4) (Evans et al., 2023).

4.4 | Short-term versus long-term changes in proglacial areas

Bennett and Evans (2012) assessed the dynamics of the Kviárjökull foreland on a decadal temporal scale based on DEMs generated from aerial images taken in the period 1945–2003, generating four DoDs for the periods: 1945–1964, 1964–1980, 1980–1998 and 1998–2003. They identified the fact that elevation changes in the ice-cored moraine complex did not proceed at the same rate. Changes in the average annual thickness decreased during the first three periods (−0.8 m a^{-1} in 1945–1964, −0.3 m a^{-1} in 1964–1980 and 0.015 m a^{-1} in 1980–1998) and then started to slightly increase in the fourth period (0.044 m a^{-1} in 1998–2003). Positive values in the period 1980–1998 were a result of snout readvance into ice-cored terrain as a response to the 1990s readvance event in southern Iceland (sensu Evans & Hiemstra, 2005; Sigurðsson, 2005; Bradwell et al., 2006; Sigurðsson et al., 2007; Evans & Chandler, 2018). The results of our more recent, short-term calculations reveal that the trend of increasing rates of change for the period 1998–2003 have been sustained, with all the case study areas exceeding the average change in annual thickness of 0.044 m a^{-1} recorded by Bennett and Evans (2012) for the period 1998–2003 (Figure 11). These results are similar to those from other long-term analyses. For example, on the foreland of Ragnarbreen, Svalbard, the average annual change in elevation in the period 1961–2009 was −0.033 m a^{-1} (Ewertowski, 2014). Additionally, on the Hørbyebreen foreland, Svalbard, ground surface elevation changed annually on average by −0.15 m a^{-1} throughout the period 1960–2009, with an average maximum volume change of −1.3 m a^{-1} (Ewertowski et al., 2019). On the foreland of Brúarjökull, Iceland, there was an average ground surface change from −0.10 to −0.18 m a^{-1} over the period 1945–2005 (Schomacker & Kjaer, 2007) and on the Kötlujökull foreland, Iceland, ice-cored moraine surfaces dropped on average annually from −0.3 to −1.4 m a^{-1} in 1995–1998 (Krüger & Kjær, 2000). A similarly high level of activity has been reported for the ice-cored moraine on the foreland of Holmströmbreen, Svalbard, by Schomacker and Kjaer (2008), with a mean annual surface change of −0.9 m a^{-1} for the period 1984–2004 (similar to our case study area 3 at −0.82 m a^{-1} for the period 2014–2022).

4.5 | Degradation of an ice-cored moraine complex—implications for the interpretation of Pleistocene landforms and sediments

The four case study areas analysed here constitute land elements within the debris-charged, active temperate glacial landsystem at Kviárjökull (Bennett et al., 2010), the evolution of which are presented in Figures 1c and 12. This provides an overview of landsystem development over the longer timescale of 1945–2014 (Figure 12), during which the kame terrace staircase (area 1), the outwash plain (area 2), the ice-cored hummocky moraine complex (area 3) and the ice-cored hummocky terrain with discontinuous sinuous ridges (area 4) have emerged and evolved on the northern half of the glacier foreland. In the wider context of the foreland, these land elements constitute the landform–sediment assemblages of an outwash head that has developed over the adverse slope of an overdeepening (Bennett & Evans, 2012; Spedding & Evans, 2002). This is a landsystem signature that is becoming more widely recognized on the rapidly evolving forelands of the southern Iceland temperate outlet glaciers, where high ice mass turnover and concomitant high meltwater discharges have given rise to substantial accumulations of glacifluvial sediments widely deposited over downwasting but active snouts (Bennett & Evans, 2012; Chandler, Evans, et al., 2020; Evans et al., 2018, 2019, 2023; Evans & Orton, 2015). Long-term meltwater drainage towards the outwash head can be reconstructed based on the repeat aerial imagery since 1945 and this has facilitated a much improved

TABLE 4 Comparison of glacial landform degradation rates in different sites in Iceland and Svalbard.

Location	Landform	Observation period	Annual average elevation change (m a^{-1})	Average maximum elevation change (m a^{-1})	Source
Short-term surveys (days to annual)					
Midtre Lovénbreen, Svalbard	Ice-cored moraine	2003–2005	−0.65	N/A	Irvine-Fynn et al. (2011)
Ragnarbreen, Svalbard	Ice-cored moraine	2012–2014	−0.14	−1.0	Ewertowski and Tomczyk (2015)
Ebbabreen, Svalbard	Ice-cored moraine	2012–2014	−1.83	−7.9	Ewertowski and Tomczyk (2015)
Fjallsjökull, Iceland	Ice-cored moraine	2016–2019	N/A	−6.0	Chandler, Evans, et al. (2020)
Fjallsjökull, Iceland	South overdeepening, including	2014–2022	−0.15	−1.94	Evans et al. (2023)
	(a) Large esker network	2014–2022	−0.08	−1.19	
	(b) Inner overdeepening (hummocky terrain)	2014–2022	−0.63	−1.94	
	(c) Adverse slope	2014–2022	−0.25	−1.13	
	(d) Outer overdeepening	2014–2022	0.00	N/A	
Hrútárjökull, Iceland	1990s thrust moraine	2014–2022	−0.96	−1.94	Evans et al. (2023)
Hrútárjökull, Iceland	Overdeepening	2014–2022	−0.79	−3.69	Evans et al. (2023)
Hrútárjökull, Iceland	Hummocky terrain/medial moraine	2014–2022	−0.51	N/A	Evans et al. (2023)
Hrútárjökull, Iceland	Collapsed sandur	2014–2022	−0.46	−1.87	Evans et al. (2023)
Hrútárjökull, Iceland	Debris-covered snout	2019–2022	−1.33	−8.5	Evans et al. (2023)
Kviárjökull, Iceland	Kame terrace staircase	2014–2022	−0.13	−1.43	This study
Kviárjökull, Iceland	Outwash plain	2016–2022	−0.29	−1.02	This study
Kviárjökull, Iceland	Ice-cored hummocky moraine complex	2014–2022	−0.82	−2.96	This study
Kviárjökull, Iceland	Ice-cored hummocky terrain	2016–2022	−0.26	−1.60	This study
Long-term surveys (decadal)					
Austre Lovénbreen, Svalbard	Ice-cored moraine	2003–2014	−0.13	−0.36	Tonkin et al. (2016)
Midtre Lovénbreen, Svalbard	Frontal moraine (limited buried ice content)	2003–2014	−0.09	N/A	Midgley et al. (2018)
Midtre Lovénbreen, Svalbard	Lateral moraine (ice-proximal slope)	2003–2014	−0.06	N/A	Midgley et al. (2018)
Midtre Lovénbreen, Svalbard	Medial moraine (ice-cored)	2003–2014	−0.40	N/A	Midgley et al. (2018)
Midtre Lovénbreen, Svalbard	Outwash plain	2003–2014	−0.02	N/A	Midgley et al. (2018)
Midtre Lovénbreen, Svalbard	Hummocky moraine	2003–2014	−0.03	N/A	Midgley et al. (2018)
Holmströmbreen, Svalbard	Ice-cored moraine	1984–2004	−0.9	N/A	Schomacker and Kjaer (2008)
Ragnarbreen, Svalbard	Ice-cored moraine	1961–2009	−0.033	−0.24	Ewertowski (2014)
Hørbyebreen, Svalbard	Ice-cored moraine	1960–2009	−0.15	−1.30	Ewertowski et al. (2019)
Brúarjökull, Iceland	Ice-cored moraine	1945–2005	−0.10 to −0.18	N/A	Schomacker and Kjaer (2007)
Kötlujökull, Iceland	Ice-cored moraine	1995–1998	−0.3 to −1.4	N/A	Krüger and Kjær (2000)
Kviárjökull, Iceland	Ice-cored moraine complex	1945–1964	−0.8	N/A	Bennett and Evans (2012)
		1964–1980	−0.3	N/A	
		1980–1998	−0.015	N/A	
		1998–2003	−0.044	N/A	

understanding of englacial drainage pathways through snouts overlying overdeepenings (Figure 12).

Meltwater drainage towards the apex of the outwash head was clearly fed by a portal in the centre of the glacier snout but it was not obvious until the capture of 1964 imagery where the lake water centred over study area 2 in 1945 was draining away. This becomes apparent in the emergence of englacial eskers in the debris covered snout on the 1964 and 1980 imagery (Figure 12). An esker origin for these ridges is verified by their field characteristics of well-sorted stratified gravels and sands (Bennett & Evans, 2012; Spedding & Evans, 2002). After lake drainage, meltwater streams flowing over the kame terraces (area 1) to form the outwash plain (area 2) disappeared under the snout margin, emerging again on the northern part of the outwash head apex in 1964 (Figure 12). By 1980, this meltwater pathway through the snout becomes more obvious where an N-S trending stream draining through ice-cored terrain is clearly feeding the active apex of the outwash head at the centre of the snout. The emergence of englacial eskers is manifested in the imagery of the ice-cored moraine complex (area 3) by the appearance of sinuous ridges. These ridges document drainage through the ice in a NW-SE direction prior to 1980, constituting 'engorged eskers' (sensu Mannerfelt, 1945, 1949; Evans et al., 2018). However, later imagery from 2012 shows W-E–orientated ridges, likely documenting the drainage through the glacitectonic thrust mass constructed in the 1990s, towards the meltwater stream that was established around the front of the thrust mass at that time and visible on the 1998 imagery (Figure 12). By 2022, our UAV imagery reveals the emergence of a further set of englacial eskers in the lower part of the collapsing ice-cored moraine complex and aligned ENE-WSW (Figure 13). Drainage towards the higher topography in the ENE seems unlikely, especially as these eskers would have accumulated in tunnels cut through lower elevation ice after thrust mass construction. Consequently, we envisage their production by meltwater drainage away from the extensive collapsed terrain that has developed beneath the eastern end of the outwash plain and towards the contemporary proglacial lake. If correct, this interpretation highlights the development of 'engorged eskers', but of a type that is driven by a groundwater hydrology scenario in which water pressures are not glacier induced. Moreover, drainage directions are the reverse of those that would be reconstructed based solely on landform evidence in a fully deglaciated landscape. Additionally, eskers have developed at different levels within a downwasting glacier mass as a result of two entirely different 'engorged' drainage scenarios.

In addition to the unusually complex esker development, the ice-cored moraine complex (case study area 3) is an excellent example of a terrain produced by incremental stagnation of a debris-covered snout that was subsequently glacitectonically pushed by glacier readvance during the 1990s (Figures 1b, 12 and 13; Bennett and Evans (2012)). Arcuate ridges were constructed at the eastern end of the moraine complex, comprising compressed and thrust stacked ice-cored ridges and eskers, which were gradually emerging through the debris-covered snout prior to the readvance. This is an ice-cored version of a composite glacitectonic thrust moraine (sensu Aber et al., 1989). The inclusion of buried glacier ice in the thrust mass has significant implications for glacial geomorphology in that de-icing will result in the gradual destruction of linearity and a final landform that resembles hummocky terrain rather than a recognizable glacitectonic thrust mass. In 2014 and 2016 imagery, the arcuate ridges diagnostic of thrust mass construction was still visible despite the significant mass lost through de-icing (Figure 13). Since 2014, however, downwasting due to de-icing has gradually fragmented the linearity and this has been replaced by increasing amounts of chaotic hummocky and pitted terrain as well as the ESE-WNW engorged eskers.

The historical development of the ice-cored hummocky terrain with discontinuous sinuous ridges (area 4) not only serves as an excellent genetic model for outwash heads but also provides insight into the operation of glacial meltwater pathways over overdeepenings. Like study area 3, this area appeared as ice-cored, pitted terrain at the elongate apex of the main proglacial outwash fan in 1980, but was glacitectonically compressed to form an ice-cored composite thrust mass fronted by push ridges in glacifluvial deposits during the 1990s readvance (Figures 1c and 12). As it then downwasted into hummocky terrain, it was also incised and reworked in several places by glacial meltwater streams existing from portals on the glacier snout. Associated with the portal positions have been sinuous ridges composed of well-sorted and stratified gravels and sands emerging from the downwasting ice-cored terrain over time. These ridges are interpreted as englacial eskers due to their continuation onto the glacier surface and their clear emergence from englacial positions (Bennett et al., 2010; Bennett & Evans, 2012; Spedding & Evans, 2002). The association of the eskers with an ice-cored proglacial outwash fan clearly demonstrates that the majority of the meltwater draining through the glacier snout has bypassed the floor of the overdeepening, explaining the very restricted occurrence of supercooled ice (Larson et al., 2010; Roberts et al., 2002; Spedding & Evans, 2002; Swift et al., 2006).

4.6 | Problems and limitations in using data collected with optical sensors on UAVs

While the use of UAVs in glacial geomorphology increased rapidly after 2015 (see Śledź et al., 2021), data processing results are not free of artefacts and can exhibit problems, which require careful investigations in order to avoid erroneous interpretation. The most common issues associated with SfM reconstruction are related to water surfaces, which are particularly important in rapidly changing glacier forelands prone to high levels of de-icing and concomitant pond and lake development, growth and decay. For example, SfM can reconstruct points located underwater in shallow, transparent ponds (Carrivick & Smith, 2019); however, the algorithm struggles in cases with high water turbidity or suspended sediments (see Tomczyk & Ewertowski, 2021). In our case studies, this was clearly the case in relation to the large proglacial/supraglacial lake, which was characterized by high suspended sediment concentrations combined with small wind-generated ripples, resulting in the erroneous reconstruction of the water surface. To avoid the impact of these errors on DoD

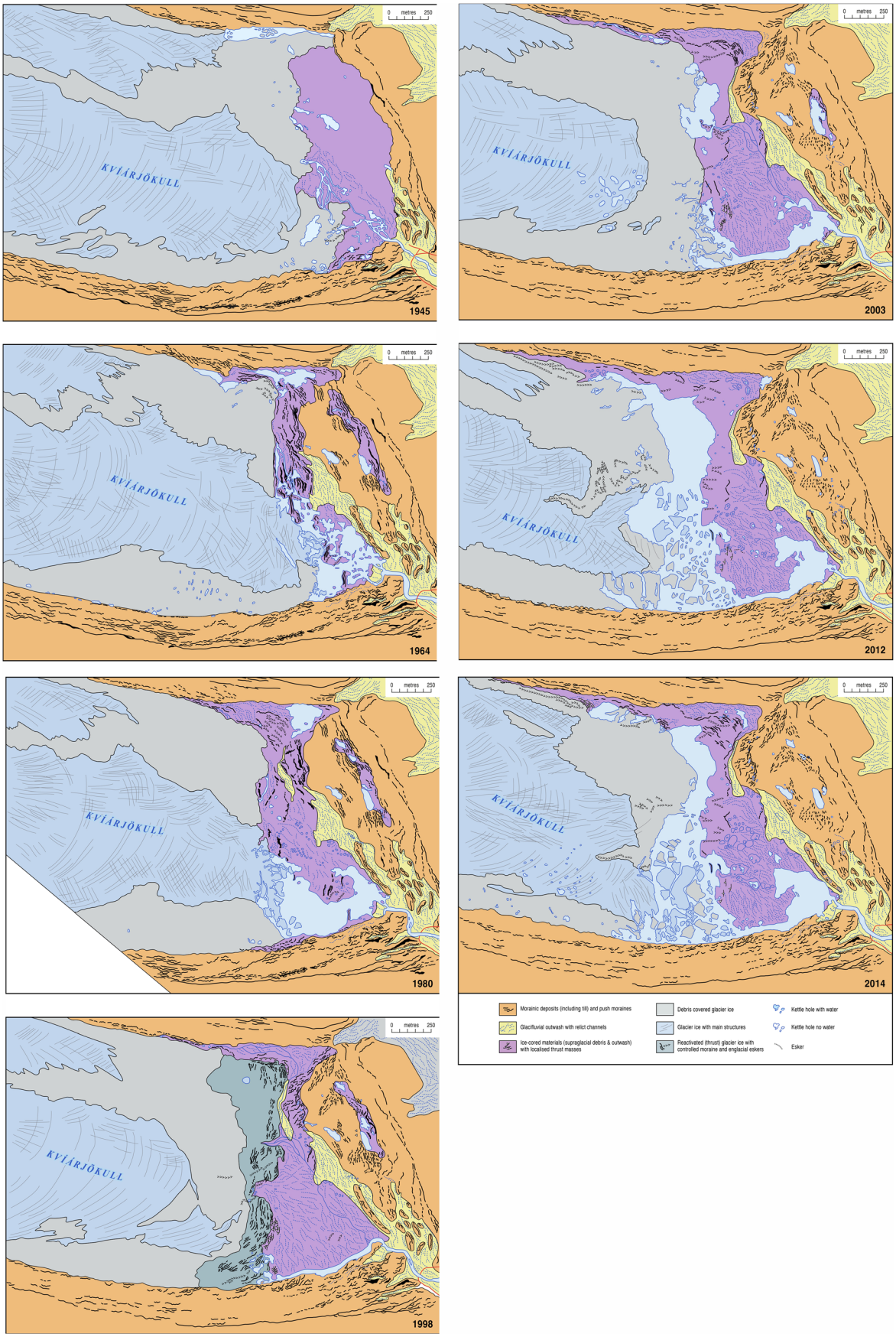

FIGURE 12 Legend on next page.

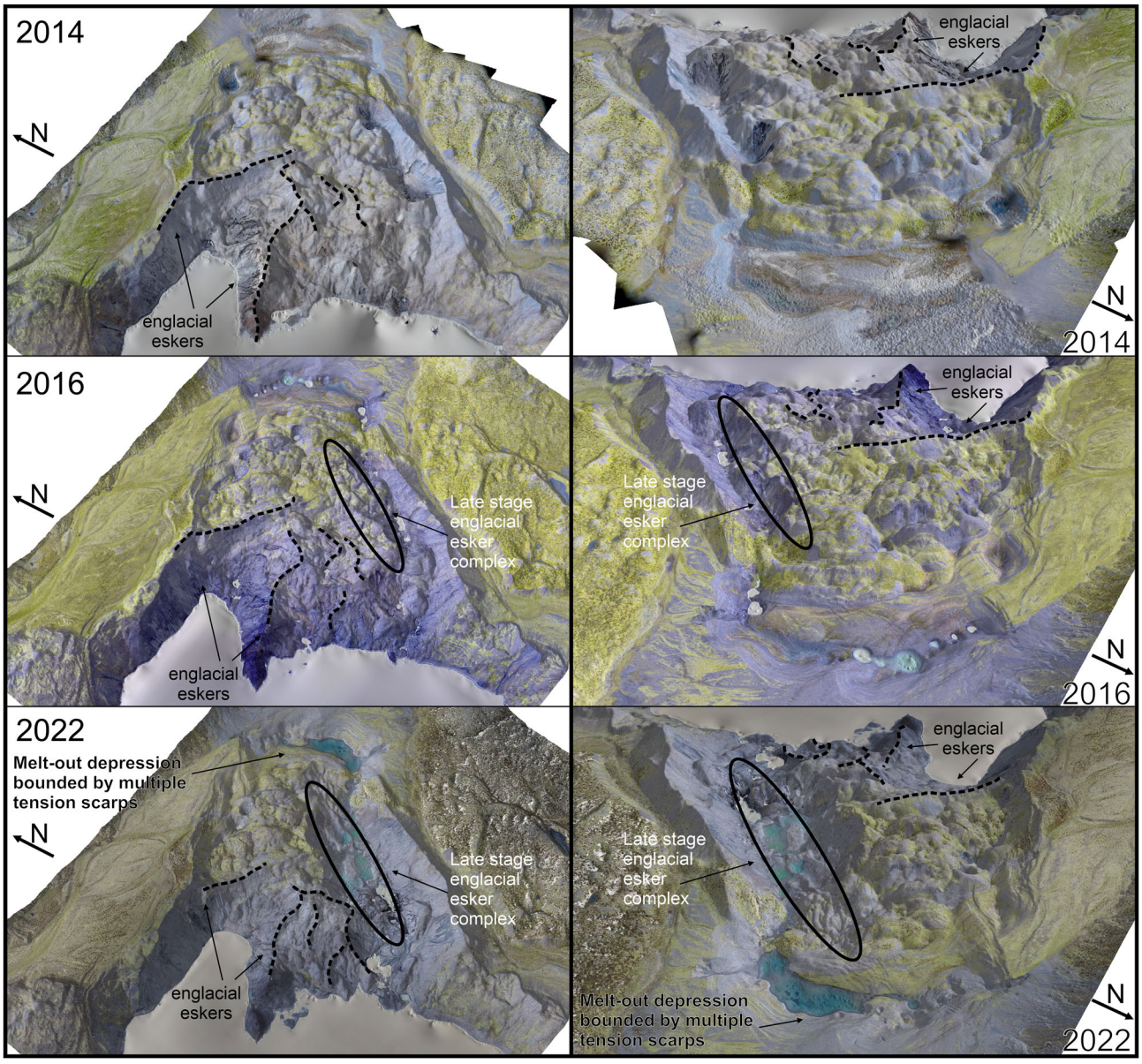

FIGURE 13 3D visualizations of the ice-cored moraine complex (see Figure 2 for location) between 2014 and 2022 illustrating different stages of degradation and the emergence of englacial eskers. [Colour figure can be viewed at wileyonlinelibrary.com]

calculations, points characterized by high uncertainty (e.g., located only on two images) were removed from the dense point cloud and a smooth water surface was thereby created (Figure 14a). Moreover, borders of case studies were delineated to avoid the lake area (Figure 2). In the case of minor, transparent waterbodies, depending on the water depth, underwater terrain was reconstructed to some extent, but in some cases erroneous points were generated and this impacted on elevation and shading models (Figure 14b). In such cases, the careful examination of not only DEMs but also orthomosaics is required.

Indeed, the investigation of different products of SfM (point clouds, DEMs and orthomosaics), in combination with field verification, is crucial for accurate interpretations of geomorphological process–form regimes. For example, in our case study area 2 (outwash plain), a 192 m^3 increase in the volume was recorded for the 2021–2022 period (Figures 7b and 11, Tables 2, 4 and 5) but the analysis of

FIGURE 12 Palaeogeographic reconstructions of glacier change and landform development for the debris-charged, active temperate foreland at Kviárjökull based on aerial imagery (1945–2003) and high-resolution satellite imagery (2012–2014). [Colour figure can be viewed at wileyonlinelibrary.com]

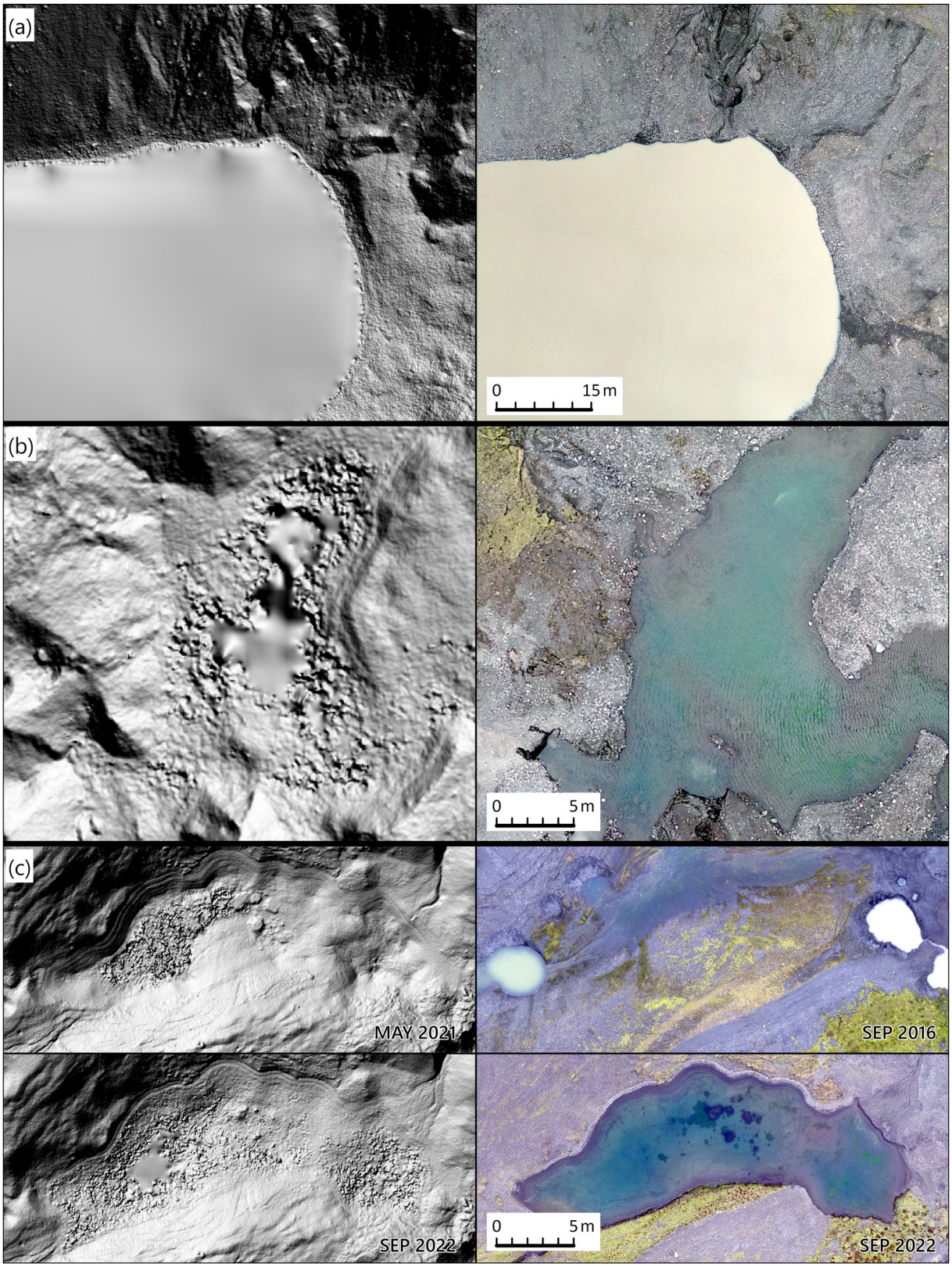

FIGURE 14 Examples of problems with data processing encountered in the study area: (a) lake with a high concentration of suspended sediments which required filtration of the point cloud; (b) small transparent waterbodies, which generated erroneous surfaces and (c) depression filled with water, which was responsible for an increase in volume recorded by DoD. [Colour figure can be viewed at wileyonlinelibrary.com]

TABLE 5 Average annual volume change for each case study.

DoD	Average annual volume change (m^3)
Case study 1	
September 2014–September 2021	−932.92
September 2021–May 2022	−44.46
Total (September 2014–May 2022)	−834.99
Case study 2	
September 2016–September 2021	−3130.12
September 2021–May 2022	289.14
Total (September 2016–May 2022)	−2724.74
Case study 3	
September 2014–September 2016	−45,091.83
September 2016–September 2021	−51,299.21
September 2021–May 2022	−25,811.33
Total (September 2014–May 2022)	−47,709.52
Case study 4	
September 2016–September 2021	−12,065.66
September 2021–May 2022	−2777.67
Total (September 2016–May 2022)	−11,405.57

Note: DEMs of differencs (DoDs) for 09.2021–05.2022 mainly cover winter period, so average values are much lower than in other periods.

orthomosaics indicated that the elevation increase was not related to landform change, but instead to the water that filled the depression over time (Figure 14c).

5 | CONCLUSIONS

This study investigated landform transformation in relation to the development of the debris-charged temperate glacial landsystem on the foreland of Kviárjökull, SE Iceland, for the period 1945–2022, with high-resolution quantification of surface change resulting from de-icing over the period 2014–2022. Observations were based on aerial photograph archives, high-resolution satellite imagery and a time series of UAV-gathered data. UAV images were processed using the SfM approach to generate DEMs, which were then used to develop the DoDs and perform the change detection. We selected four case study areas representative of specific landform elements, including a kame terrace staircase, an outwash plain, an ice-cored hummocky moraine complex and an ice-cored hummocky terrain with discontinuous sinuous ridges (englacial eskers). The recorded short-term dynamics of the landform changes at Kviárjökull are consistent with those reported at other rapidly deglaciating forelands in the northern polar region. The average annual change in volume as derived from land surface lowering ranged from −0.06 m a^{-1} in a relatively stable area of kame terrace staircase to −0.82 m a^{-1} for the ice-cored hummocky moraine complex. Compared with long-term research in this foreland since 1945, our results confirm the ongoing degradation of ice-cored moraine and outwash complexes, visible and quantifiable by using land surface collapse, at variable rates related to buried ice volume and age of deglaciation. The gradual evolution of largely chaotic hummocky terrain from not only debris-covered glacier ice but also from glacitectonic thrust masses, outwash fans/heads and complex englacial esker networks is an important modern landsystem analogue for informing palaeoglaciological reconstructions in areas characterized by hummocky 'moraine' and/or kame and kettle topography.

ACKNOWLEDGMENTS

This research was funded by the National Science Centre, Poland, grant number 2019/35/B/ST10/03928. Scientific research permits for the fieldwork were kindly provided by the Vatnajökull National Park and the Icelandic Research Council (RANNIS).

CONFLICT OF INTEREST STATEMENT

The authors declare that they have no conflict of interest.

DATA AVAILABILITY STATEMENT

The data that support the findings of this study are available from the corresponding author upon reasonable request.

ORCID

Szymon Śledź https://orcid.org/0000-0002-4822-7568
Marek W. Ewertowski https://orcid.org/0000-0002-0422-2327

REFERENCES

Aber, J. S., Croot, D. G., & Fenton, M. M. (1989). *Glaciotectonic landforms and structures*. Springer Science+Business Media.

Allen, C. D., Macalady, A. K., Chenchouni, H., Bachelet, D., McDowell, N., Vennetier, M., Kitzberger, T., Rigling, A., Breshears, D. D., Hogg, E. H., Gonzalez, P., Fensham, R., Zhang, Z., Castro, J., Demidova, N., Lim, J.-H., Allard, G., Running, S. W., Semerci, A., & Cobb, N. (2010). A global overview of drought and heat-induced tree mortality reveals emerging climate change risks for forests. *Forest Ecology and Management*, *259*(4), 660–684. https://doi.org/10.1016/j.foreco.2009.09.001

Bash, E., Moorman, B., & Gunther, A. (2018). Detecting short-term surface melt on an Arctic glacier using UAV surveys. *Remote Sensing*, *10*(10), 1547. https://doi.org/10.3390/rs10101547

Bash, E. A., & Moorman, B. J. (2020). Surface melt and the importance of water flow – An analysis based on high-resolution unmanned aerial vehicle (UAV) data for an Arctic glacier. *The Cryosphere*, *14*(2), 549–563. https://doi.org/10.5194/tc-14-549-2020

Benn, D. I., Bolch, T., Hands, K., Gulley, J., Luckman, A., Nicholson, L. I., Quincey, D., Thompson, S., Toumi, R., & Wiseman, S. (2012). Response of debris-covered glaciers in the Mount Everest region to recent warming, and implications for outburst flood hazards. *Earth-Science Reviews*, *114*(1–2), 156–174. https://doi.org/10.1016/j.earscirev.2012.03.008

Benn, D. I., & Evans, D. J. A. (2010). *Glaciers and glaciation*. Hodder Education.

Bennett, G. L., & Evans, D. J. A. (2012). Glacier retreat and landform production on an overdeepened glacier foreland: The debris-charged glacial landsystem at Kviárjökull, Iceland. *Earth Surface Processes and Landforms*, *37*(15), 1584–1602. https://doi.org/10.1002/esp.3259

Bennett, G. L., Evans, D. J. A., Carbonneau, P., & Twigg, D. R. (2010). Evolution of a debris-charged glacier landsystem, Kviárjökull, Iceland. *Journal of Maps*, *6*(1), 40–67. https://doi.org/10.4113/jom.2010.1114

Bernard, É., Friedt, J. M., Tolle, F., Marlin, C., & Griselin, M. (2016). Using a small COTS UAV to quantify moraine dynamics induced by climate shift in Arctic environments. *International Journal of Remote Sensing*, *38*(8–10), 2480–2494. https://doi.org/10.1080/01431161.2016.1249310

Blauvelt, D. J., Russell, A. J., Large, A. R. G., Tweed, F. S., Hiemstra, J. F., Kulessa, B., Evans, D. J. A., & Waller, R. I. (2020). Controls on jökulhlaup-transported buried ice melt-out at Skeiðarársandur, Iceland: Implications for the evolution of ice-marginal environments. *Geomorphology*, *360*, 107164. https://doi.org/10.1016/j.geomorph.2020.107164

Bradwell, T., Dugmore, A. J., & Sugden, D. E. (2006). The little ice age glacier maximum in Iceland and the North Atlantic oscillation: Evidence from Lambatungnajökull, Southeast Iceland. *Boreas*, *35*(1), 61–80. https://doi.org/10.1111/j.1502-3885.2006.tb01113.x

Brunsden, D., & Thornes, J. B. (1979). Landscape sensitivity and change. *Transactions of the Institute of British Geographers NS*, *4*, 485–515.

Bühler, Y., Adams, M. S., Bösch, R., & Stoffel, A. (2016). Mapping snow depth in alpine terrain with unmanned aerial systems (UASs): Potential and limitations. *The Cryosphere*, *10*(3), 1075–1088. https://doi.org/10.5194/tc-10-1075-2016

Carrivick, J. L., Boston, C. M., King, O., James, W. H. M., Quincey, D. J., Smith, M. W., Grimes, M., & Evans, J. (2019). Accelerated volume loss in glacier ablation zones of NE Greenland, little ice age to present. *Geophysical Research Letters*, *46*(3), 1476–1484. https://doi.org/10.1029/2018GL081383

Carrivick, J. L., & Heckmann, T. (2017). Short-term geomorphological evolution of proglacial systems. *Geomorphology*, *287*, 3–28. https://doi.org/10.1016/j.geomorph.2017.01.037

Carrivick, J. L., & Smith, M. W. (2019). Fluvial and aquatic applications of structure from motion photogrammetry and unmanned aerial vehicle/drone technology. *WIREs Water*, *6*(1), e1328. https://doi.org/10.1002/wat2.1328

Carrivick, J. L., & Tweed, F. S. (2019). A review of glacier outburst floods in Iceland and Greenland with a megafloods perspective. *Earth-Science Reviews*, *196*, 102876. https://doi.org/10.1016/j.earscirev.2019.102876

Chandler, B. M. P., Chandler, S. J. P., Evans, D. J. A., Ewertowski, M. W., Lovell, H., Roberts, D. H., Schaefer, M., & Tomczyk, A. M. (2020). Sub-annual moraine formation at an active temperate Icelandic glacier. *Earth Surface Processes and Landforms*, *45*(7), 1622–1643. https://doi.org/10.1002/esp.4835

Chandler, B. M. P., Evans, D. J. A., Chandler, S. J. P., Ewertowski, M. W., Lovell, H., Roberts, D. H., Schaefer, M., & Tomczyk, A. M. (2020). The glacial landsystem of Fjallsjökull, Iceland: Spatial and temporal evolution of process-form regimes at an active temperate glacier. *Geomorphology*, *361*, 107192. https://doi.org/10.1016/j.geomorph.2020.107192

Cook, K. L., Andermann, C., Gimbert, F., Adhikari, B. R., & Hovius, N. (2018). Glacial lake outburst floods as drivers of fluvial erosion in the Himalaya. *Science*, *362*(6410), 53–57. https://doi.org/10.1126/science.aat4981

Cook, S. J., Kougkoulos, I., Edwards, L. A., Dortch, J., & Hoffmann, D. (2016). Glacier change and glacial lake outburst flood risk in the Bolivian Andes. *The Cryosphere*, *10*(5), 2399–2413. https://doi.org/10.5194/tc-10-2399-2016

Etzelmüller, B. (2000). Quantification of thermo-erosion in pro-glacial areas – examples from Svalbard. *Zeitschrift Fur Geomorphologie*, *44*(3), 343–361.

Evans, D. J. A. (Ed.). (2003). *Glacial Landsystems*. Arnold.

Evans, D. J. A. (2013). The glacial and periglacial research – Geomorphology and retreating glaciers. In J. Shroder, R. Giardino, & J. Harbor (Eds.), *Glacial and periglacial geomorphology* (Vol. 8, pp. 460–478). Academic Press.

Evans, D. J. A., & Chandler, B. M. P. (2018). Geology, physiography and glaciology of SE Iceland. In D. J. A. Evans (Ed.), *Glacial landsystems of Southeast Iceland: Quaternary applications–field guide* (pp. 1–19). Quaternary Research Association.

Evans, D. J. A., Ewertowski, M. W., & Orton, C. (2019). The glacial landsystem of Hoffellsjökull, SE Iceland: Contrasting geomorphological signatures of active temperate glacier recession driven by ice lobe and bed morphology. *Geografiska Annaler: Series A, Physical Geography*, *101*(3), 249–276. https://doi.org/10.1080/04353676.2019.1631608

Evans, D. J. A., Ewertowski, M. W., Orton, C., & Graham, D. J. (2018). The glacial geomorphology of the ice cap piedmont lobe landsystem of east Mýrdalsjökull, Iceland. *Geosciences*, *8*(6), 194.

Evans, D. J. A., Ewertowski, M. W., Roberts, D. H., & Tomczyk, A. M. (2022). The historical emergence of a geometric and sinuous ridge network at the Hørbyebreen polythermal glacier snout, Svalbard and its use in the interpretation of ancient glacial landforms. *Geomorphology*, *406*, 108213. https://doi.org/10.1016/j.geomorph.2022.108213

Evans, D. J. A., Ewertowski, M. W., Tomczyk, A. M., & Chandler, B. M. P. (2023). Active temperate glacial landsystem evolution in association with outwash head/depositional overdeepenings. *Earth Surface Processes and Landforms*., *48*, 1573–1598. https://doi.org/10.1002/esp.5569

Evans, D. J. A., & Hiemstra, J. F. (2005). Till deposition by glacier submarginal, incremental thickening. *Earth Surface Processes and Landforms*, *30*(13), 1633–1662. https://doi.org/10.1002/Esp.1224

Evans, D. J. A., & Orton, C. (2015). Heinabergsjökull and Skalafellsjökull, Iceland: Active temperate piedmont lobe and outwash head glacial landsystem. *Journal of Maps*, *11*(3), 415–431. https://doi.org/10.1080/17445647.2014.919617

Evans, D. J. A., Shand, M., & Petrie, G. (2009). Maps of the snout and proglacial landforms of Fjallsjökull, Iceland (1945, 1965, 1998). *Scottish Geographical Journal*, *125*, 304–320.

Evans, D. J. A., & Twigg, D. R. (2002). The active temperate glacial landsystem: A model based on Breioamerkurjokull and Fjallsjokull, Iceland. *Quaternary Science Reviews*, *21*(20–22), 2143–2177.

Ewertowski, M. (2014). Recent transformations in the high-arctic glacier landsystem, ragnarbreen, svalbard. *Geografiska Annaler: Series A, Physical Geography*, *96*(3), 265–285. https://doi.org/10.1111/geoa.12049

Ewertowski, M. W., Evans, D. J. A., Roberts, D. H., Tomczyk, A. M., Ewertowski, W., & Pleksot, K. (2019). Quantification of historical landscape change on the foreland of a receding polythermal glacier, Hørbyebreen, Svalbard. *Geomorphology*, *325*, 40–54. https://doi.org/10.1016/j.geomorph.2018.09.027

Ewertowski, M. W., & Tomczyk, A. M. (2015). Quantification of the ice-cored moraines' short-term dynamics in the high-Arctic glaciers Ebbabreen and Ragnarbreen, Petuniabukta, Svalbard. *Geomorphology*, *234*, 211–227. https://doi.org/10.1016/j.geomorph.2015.01.023

Ewertowski, M. W., & Tomczyk, A. M. (2020). Reactivation of temporarily stabilized ice-cored moraines in front of polythermal glaciers: Gravitational mass movements as the most important geomorphological agents for the redistribution of sediments (a case study from Ebbabreen and Ragnarbreen, Svalbard). *Geomorphology*, *350*, 106952. https://doi.org/10.1016/j.geomorph.2019.106952

Eyles, N. (1979). Facies of supraglacial sedimentation on Icelandic and Alpine temperate glaciers. *Canadian Journal of Earth Sciences*, *16*(7), 1341–1361. https://doi.org/10.1139/e79-121

Eyles, N. (1983a). Glacial geology: A Landsystems approach. In N. Eyles (Ed.), *Glacial Geology* (pp. 1–18). Pergamon.

Eyles, N. (1983b). Modern Icelandic glaciers as depositional models for «hummocky moraine» in the Scottish highlands. In E. B. Evenson, C. Schluchter, & J. Rabassa (Eds.), *Tills and related deposits* (pp. 47–59). Balkema.

Fey, C., & Krainer, K. (2020). Analyses of UAV and GNSS based flow velocity variations of the rock glacier Lazaun (Ötztal Alps, South Tyrol, Italy). *Geomorphology*, *365*, 107261. https://doi.org/10.1016/j.geomorph.2020.107261

Flannigan, M. D., Krawchuk, M. A., de Groot, W. J., Wotton, B. M., & Gowman, L. M. (2009). Implications of changing climate for global wildland fire. *International Journal of Wildland Fire*, *18*(5), 483–507. https://doi.org/10.1071/WF08187

Fookes, P. G., Gordon, D. L., & Higginbottom, I. E. (1978). Glacial landforms, their deposits and engineering characteristics. In *The engineering behaviour of glacial materials* (pp. 18–51). University of Birmingham.

Gariano, S. L., & Guzzetti, F. (2016). Landslides in a changing climate. *Earth-Science Reviews*, *162*, 227–252. https://doi.org/10.1016/j.earscirev.2016.08.011

Groos, A. R., Bertschinger, T. J., Kummer, C. M., Erlwein, S., Munz, L., & Philipp, A. (2019). The potential of low-cost UAVs and open-source photogrammetry software for high-resolution monitoring of alpine glaciers: A case study from the Kanderfirn (Swiss Alps). *Geosciences*, *9*(8), 356. https://doi.org/10.3390/geosciences9080356

Harrison, S., Kargel, J. S., Huggel, C., Reynolds, J., Shugar, D. H., Betts, R. A., Emmer, A., Glasser, N., Haritashya, U. K., Klimeš, J., Reinhardt, L., Schaub, Y., Wiltshire, A., Regmi, D., & Vilímek, V. (2018). Climate change and the global pattern of moraine-dammed glacial lake outburst floods. *The Cryosphere*, *12*(4), 1195–1209. https://doi.org/10.5194/tc-12-1195-2018

Hedding, D. W., Erofeev, A. A., Hansen, C. D., Khon, A. V., & Abbasov, Z. R. (2020). Geomorphological processes and landforms of glacier forelands in the upper Aktru River basin (Gornyi Altai), Russia: Evidence for rapid recent retreat and paraglacial adjustment. *Journal of Mountain Science*, *17*(4), 824–837. https://doi.org/10.1007/s11629-019-5845-5

Hirabayashi, Y., Mahendran, R., Koirala, S., Konoshima, L., Yamazaki, D., Watanabe, S., Kim, H., & Kanae, S. (2013). Global flood risk under climate change. *Nature Climate Change*, *3*(9), 816–821. https://doi.org/10.1038/nclimate1911

Hugonnet, R., McNabb, R., Berthier, E., Menounos, B., Nuth, C., Girod, L., Farinotti, D., Huss, M., Dussaillant, I., Brun, F., & Kaab, A. (2021). Accelerated global glacier mass loss in the early twenty-first century. *Nature*, *592*(7856), 726–731. https://doi.org/10.1038/s41586-021-03436-z

Irvine-Fynn, T. D. L., Barrand, N. E., Porter, P. R., Hodson, A. J., & Murray, T. (2011). Recent high-Arctic glacial sediment redistribution: A process perspective using airborne lidar. *Geomorphology*, *125*(1), 27–39. https://doi.org/10.1016/j.geomorph.2010.08.012

Jouvet, G., Weidmann, Y., Kneib, M., Detert, M., Seguinot, J., Sakakibara, D., & Sugiyama, S. (2018). Short-lived ice speed-up and plume water flow captured by a VTOL UAV give insights into subglacial hydrological system of Bowdoin Glacier. *Remote Sensing of Environment*, *217*, 389–399. https://doi.org/10.1016/j.rse.2018.08.027

Jouvet, G., Weidmann, Y., van Dongen, E., Lüthi, M. P., Vieli, A., & Ryan, J. C. (2019). High-endurance UAV for monitoring calving glaciers: Application to the Inglefield Bredning and Eqip Sermia, Greenland. *Frontiers in Earth Science*, *7*, 206. https://doi.org/10.3389/feart.2019.00206

Kienholz, C., Pierce, J., Hood, E., Amundson, J. M., Wolken, G. J., Jacobs, A., Hart, S., Wikstrom Jones, K., Abdel-Fattah, D., Johnson, C., & Conaway, J. S. (2020). Deglacierization of a marginal basin and implications for outburst floods, Mendenhall glacier, Alaska. *Frontiers in Earth Science*, *8*, 137. https://doi.org/10.3389/feart.2020.00137

Kjær, K. H., & Krüger, J. (2001). The final phase of dead-ice moraine development: Processes and sediment architecture, Kotlujokull, Iceland. *Sedimentology*, *48*(5), 935–952. https://doi.org/10.1046/j.1365-3091.2001.00402.x

Knight, J., & Harrison, S. (2012a). The impacts of climate change on terrestrial Earth surface systems. *Nature Climate Change*, *3*(1), 24–29. https://doi.org/10.1038/nclimate1660

Knight, J., & Harrison, S. (2012b). Evaluating the impacts of global warming on geomorphological systems. *Ambio*, *41*(2), 206–210. https://doi.org/10.1007/s13280-011-0178-9

Knight, J., & Harrison, S. (2018). Transience in cascading paraglacial systems. *Land Degradation & Development*, *29*(6), 1991–2001. https://doi.org/10.1002/ldr.2994

Kraaijenbrink, P., Meijer, S. W., Shea, J. M., Pellicciotti, F., De Jong, S. M., & Immerzeel, W. W. (2016). Seasonal surface velocities of a Himalayan glacier derived by automated correlation of unmanned aerial vehicle imagery. *Annals of Glaciology*, *57*(71), 103–113. https://doi.org/10.3189/2016AoG71A072

Krüger, J., & Kjær, K. H. (2000). De-icing progression of ice-cored moraines in a humid, subpolar climate, Kötlujökull, Iceland. *The Holocene*, *10*(6), 737–747. https://doi.org/10.1191/09596830094980

Larson, G. J., Lawson, D. E., Evenson, E. B., Knudsen, Ó., Alley, R. B., & Phanikumar, M. S. (2010). Origin of stratified basal ice in outlet glaciers of Vatnajökull and Öræfajökull, Iceland. *Boreas*, *39*(3), 457–470. https://doi.org/10.1111/j.1502-3885.2009.00134.x

Małecki, J. (2016). Accelerating retreat and high-elevation thinning of glaciers in Central Spitsbergen. *The Cryosphere*, *10*(3), 1317–1329. https://doi.org/10.5194/tc-10-1317-2016

Małecki, J. (2022). Recent contrasting behaviour of mountain glaciers across the European High Arctic revealed by ArcticDEM data. *The Cryosphere*, *16*(5), 2067–2082. https://doi.org/10.5194/tc-16-2067-2022

Mannerfelt, C. M. (1945). Några Glacialmorfologiska Formelement. *Geografiska Annaler*, *27*(1–2), 3–5. https://doi.org/10.1080/20014422.1945.11880732

Mannerfelt, C. M. (1949). Marginal drainage channels as indicators of the gradients of quaternary ice caps. *Geografiska Annaler*, *31*(1–4), 194–199. https://doi.org/10.1080/20014422.1949.11880803

Midgley, N. G., Tonkin, T. N., Graham, D. J., & Cook, S. J. (2018). Evolution of high-Arctic glacial landforms during deglaciation. *Geomorphology*, *311*, 63–75. https://doi.org/10.1016/j.geomorph.2018.03.027

Młynarczyk, A., Konatowska, M., Królewicz, S., Rutkowski, P., Piekarczyk, J., & Kowalewski, W. (2022). Spectral indices as a tool to assess the moisture status of forest habitats. *Remote Sensing*, *14*(17), 4267. https://doi.org/10.3390/rs14174267

Nota, E. W., Nijland, W., & de Haas, T. (2022). Improving UAV-SfM time-series accuracy by co-alignment and contributions of ground control or RTK positioning. *International Journal of Applied Earth Observation and Geoinformation*, *109*, 102772. https://doi.org/10.1016/j.jag.2022.102772

Paine, A. D. M. (1985). "Ergodic" reasoning in geomorphology: Time for a review of the term? *Progress in Physical Geography*, *9*, 1–15.

Phillips, E., Everest, J., Evans, D. J. A., Finlayson, A., Ewertowski, M., Guild, A., & Jones, L. (2017). Concentrated, 'pulsed' axial glacier flow: Structural glaciological evidence from Kviárjökull in SE Iceland. *Earth Surface Processes and Landforms*, *42*(13), 1901–1922. https://doi.org/10.1002/esp.4145

Planet. (2022). Planet Application Program Interface: In Space for Life on Earth. https://api.planet.com

Price, R. J. (1969). Moraines, Sandar, Kames and Eskers near Breidamerkurjökull, Iceland. *Transactions of the Institute of British Geographers*, (46), 17–43. https://doi.org/10.2307/621406

Price, R. J. (1980). Rates of geomorphological changes in proglacial areas. In R. A. Cullingford, D. A. Davidson, & J. Lewin (Eds.), *Timescales in geomorphology* (pp. 79–93). Wiley.

Roberts, M. J., Tweed, F. S., Russell, A. J., Knudsen, O. S., Lawson, D. E., Larson, G. J., Evenson, E. B., & Björnsson, H. (2002). Glaciohydraulic supercooling in Iceland. *Geology*, *30*(5), 439–442. https://doi.org/10.1130/0091-7613(2002)030<0439:Gsii>2.0.Co;2

Rossini, M., Di Mauro, B., Garzonio, R., Baccolo, G., Cavallini, G., Mattavelli, M., De Amicis, M., & Colombo, R. (2018). Rapid melting dynamics of an alpine glacier with repeated UAV photogrammetry. *Geomorphology*, *304*, 159–172. https://doi.org/10.1016/j.geomorph.2017.12.039

Ryan, J. C., Hubbard, A. L., Box, J. E., Todd, J., Christoffersen, P., Carr, J. R., Holt, T. O., & Snooke, N. (2015). UAV photogrammetry and structure

from motion to assess calving dynamics at Store Glacier, a large outlet draining the Greenland ice sheet. *The Cryosphere*, *9*(1), 1–11. https://doi.org/10.5194/tc-9-1-2015

Schomacker, A. (2008). What controls dead-ice melting under different climate conditions? A discussion. *Earth-Science Reviews*, *90*(3–4), 103–113. https://doi.org/10.1016/j.earscirev.2008.08.003

Schomacker, A., & Kjaer, K. H. (2007). Origin and de-icing of multiple generations of ice-cored moraines at Bruarjokull, Iceland. *Boreas*, *36*(4), 411–425. https://doi.org/10.1080/03009480701213554

Schomacker, A., & Kjær, K. H. (2008). Quantification of dead-ice melting in ice-cored moraines at the high-Arctic glacier Holmströmbreen, Svalbard. *Boreas*, *37*(2), 211–225. https://doi.org/10.1111/j.1502-3885.2007.00014.x

Seier, G., Kellerer-Pirklbauer, A., Wecht, M., Hirschmann, S., Kaufmann, V., Lieb, G. K., & Sulzer, W. (2017). UAS-based change detection of the glacial and proglacial transition zone at Pasterze glacier, Austria. *Remote Sensing*, *9*(6), 549. https://doi.org/10.3390/rs9060549

Sigurðsson, O. (2005). Variations of termini of glaciers in Iceland in recent centuries and their connection with climate. In C. Caseldine, A. Russell, J. Harðardóttir, & Ó. Knudsen (Eds.), *Developments in quaternary sciences* (Vol. 5, pp. 241–255). Elsevier.

Sigurðsson, O., Jónsson, T., & Jóhannesson, T. (2007). Relation between glacier-termini variations and summer temperature in Iceland since 1930. *Annals of Glaciology*, *46*, 170–176. https://doi.org/10.3189/172756407782871611

Śledź, S., & Ewertowski, M. W. (2022). Evaluation of the influence of processing parameters in structure-from-motion software on the quality of digital elevation models and orthomosaics in the context of studies on earth surface dynamics. *Remote Sensing*, *14*(6), 1312. https://doi.org/10.3390/rs14061312

Śledź, S., Ewertowski, M. W., & Piekarczyk, J. (2021). Applications of unmanned aerial vehicle (UAV) surveys and structure from motion photogrammetry in glacial and periglacial geomorphology. *Geomorphology*, *378*, 107620. https://doi.org/10.1016/j.geomorph.2021.107620

Song, X. P., Hansen, M. C., Stehman, S. V., Potapov, P. V., Tyukavina, A., Vermote, E. F., & Townshend, J. R. (2018). Global land change from 1982 to 2016. *Nature*, *560*(7720), 639–643. https://doi.org/10.1038/s41586-018-0411-9

Spedding, N., & Evans, D. J. A. (2002). Sediments and landforms at Kviarjokull, Southeast Iceland: A reappraisal of the glaciated valley landsystem. *Sedimentary Geology*, *149*(1–3), 21–42.

Staines, K. E. H., & Carrivick, J. L. (2015). Geomorphological impact and morphodynamic effects on flow conveyance of the 1999 jökulhlaup at sólheimajökull, Iceland. *Earth Surface Processes and Landforms*, *40*(10), 1401–1416. https://doi.org/10.1002/esp.3750

Staines, K. E. H., Carrivick, J. L., Tweed, F. S., Evans, A. J., Russell, A. J., Jóhannesson, T., & Roberts, M. (2015). A multi-dimensional analysis of pro-glacial landscape change at Sólheimajökull, southern Iceland. *Earth Surface Processes and Landforms*, *40*(6), 809–822. https://doi.org/10.1002/esp.3662

Strzelecki, M. C., Long, A. J., Lloyd, J. M., Małecki, J., Zagórski, P., Pawłowski, Ł., & Jaskólski, M. W. (2018). The role of rapid glacier retreat and landscape transformation in controlling the post-Little Ice Age evolution of paraglacial coasts in Central Spitsbergen (Billefjorden, Svalbard). *Land Degradation & Development*, *29*(6), 1962–1978. https://doi.org/10.1002/ldr.2923

Swift, D. A., Evans, D. J. A., & Fallick, A. E. (2006). Transverse englacial debris-rich ice bands at Kviárjökull, Southeast Iceland. *Quaternary Science Reviews*, *25*(13), 1708–1718.

Sziło, J., & Bialik, R. (2018). Recession and ice surface elevation changes of Baranowski glacier and its impact on proglacial relief (King George Island, West Antarctica). *Geosciences*, *8*(10), 355. https://doi.org/10.3390/geosciences8100355

Tomczyk, A. M., & Ewertowski, M. W. (2021). Baseline data for monitoring geomorphological effects of glacier lake outburst flood: A very-high-resolution image and GIS datasets of the distal part of the Zackenberg River, Northeast Greenland. *Earth System Science Data*, *13*(11), 5293–5309. https://doi.org/10.5194/essd-13-5293-2021

Tomczyk, A. M., Ewertowski, M. W., & Carrivick, J. L. (2020). Geomorphological impacts of a glacier lake outburst flood in the high arctic Zackenberg River, NE Greenland. *Journal of Hydrology*, *591*, 125300. https://doi.org/10.1016/j.jhydrol.2020.125300

Tonkin, T. N., Midgley, N. G., Cook, S. J., & Graham, D. J. (2016). Ice-cored moraine degradation mapped and quantified using an unmanned aerial vehicle: A case study from a polythermal glacier in Svalbard. *Geomorphology*, *258*, 1–10. https://doi.org/10.1016/j.geomorph.2015.12.019

van der Sluijs, J., Kokelj, S., Fraser, R., Tunnicliffe, J., & Lacelle, D. (2018). Permafrost terrain dynamics and infrastructure impacts revealed by UAV photogrammetry and thermal imaging. *Remote Sensing*, *10*(11), 1734. https://doi.org/10.3390/rs10111734

van Woerkom, T., Steiner, J. F., Kraaijenbrink, P. D. A., Miles, E. S., & Immerzeel, W. W. (2019). Sediment supply from lateral moraines to a debris-covered glacier in the Himalaya. *Earth Surface Dynamics*, *7*(2), 411–427. https://doi.org/10.5194/esurf-7-411-2019

Westoby, M. J., Brasington, J., Glasser, N. F., Hambrey, M. J., & Reynolds, J. M. (2012). 'Structure-from-Motion' photogrammetry: A low-cost, effective tool for geoscience applications. *Geomorphology*, *179*, 300–314. https://doi.org/10.1016/j.geomorph.2012.08.021

Westoby, M. J., Rounce, D. R., Shaw, T. E., Fyffe, C. L., Moore, P. L., Stewart, R. L., & Brock, B. W. (2020). Geomorphological evolution of a debris-covered glacier surface. *Earth Surface Processes and Landforms*, *45*(14), 3431–3448. https://doi.org/10.1002/esp.4973

Wheaton, J. M., Brasington, J., Darby, S. E., & Sear, D. A. (2010). Accounting for uncertainty in DEMs from repeat topographic surveys: Improved sediment budgets. *Earth Surface Processes and Landforms*, *35*(2), 136–156. https://doi.org/10.1002/esp.1886

How to cite this article: Śledź, S., Ewertowski, M. W., & Evans, D. J. A. (2023). Quantification of short-term transformations of proglacial landforms in a temperate, debris-charged glacial landsystem, Kviárjökull, Iceland. *Land Degradation & Development*, *34*(17), 5566–5590. https://doi.org/10.1002/ldr.4865